20th FERROFLUIDWORKSHOP

Benediktbeuern

September 25th - 27th 2024

Program Overview

Opening	25.09.2024	13:30 – 13:50
Session 1		13:50 – 15:50
Coffee Break		15:50 – 16:20
Session 2		16:20 – 18:20
Postersession		18:20 – 20:00
Walking / Bus Tour	26.09.2024	08:30 – 16:00
Mountain Talks		
Winners of the Doctoral Thesis Award		17:00 – 18:30
Workshop-Dinner		19:00 - …
Session 3	27.09.2024	08:40 – 10:00
Coffee Break		10:00 – 10:30
Session 4		10:30 – 12:10
Closing		12:15 – 12:30

next trains to Munich will leave 13:02 and 13:58

Content

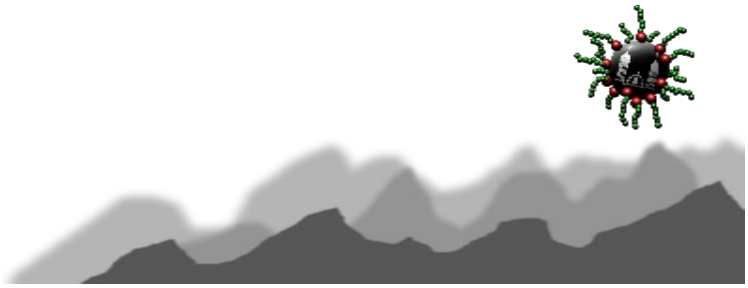

Wedensday, September 25th

13:30	***Opening***	
13:50	**Session 1**	
13:50 – 14:10	J. Kirchner	*Superparamagnetic Nanoparticles in Magnetic Drug Targeting and Molecular Communication*
14:10 – 14:30	C. M. Huber, H. Ermert, I. Ullmann, M. Vossiek, C. Alexiou, S. Lyer	*Ultrasound-based Methods for Imaging Superparamagnetic Iron Oxide Nanoparticles in Biomedical Applications*
14:30 – 14:50	A. Weidner, D. Eberbeck, S. Dutz	*Influence of light irradiation on Iron Oxide Nanoparticles*
14:50 – 15:10	A. Nasser, A. Qdemat, H. Unterweger, R. Tietze, X. Sun, J. Landers, J. Kopp, B. Wu, M.-S. Appavou, A. Murmiliuk, E.P. Gilbert, O. Petracic, A. Feoktystov	*Impact of Coating Type on Structure and Magnetic Properties of Biocompatible Iron Oxide Nanoparticles: Insights into Cluster Organization and Oxidation Behaviour*
15:10 – 15:30	D. Eberbeck, F. Wiekhorst	*Increase of MPS signal by isotropic aggregates of magnetic nanoparticles*
15:30 – 15:50	F. Wolgast, E. Wendt, M. Schilling, F. Ludwig, T. Viereck	*Magnetic Particle Spectroscopy measurements with adjustable DC offset fields*
15:50	***Coffee break & Posters***	

16:20	**Session 2**	
16:20 – 16:40	I. Rehberg, P. Blümler, E. Aderhold, Th. Friedrich	*Scrutinizing magnetic fields of dipole clusters*
16:40 – 17:00	M. Krichler, S. Odenbach	*Particle interaction in heat transfer in ferrofluids*
17:00 – 17:20	M. Reiche, L. Zentner, D. Borin, T.I. Becker	*Vibration-driven planar motion system based on multipole magnetoactive elastomers*
17:20 – 17:40	A. Lakkis, O. Bilous, P.A. Sanchez, S.S. Kantorovich, R. Richter	*Coarsening Dynamics of Ferromagnetic Granular Networks Under Variation of the Acceleration Amplitude*
17:40 – 18:00	Noorjahan	*Investigate the Polyaniline decorated Iron based Magnetorheological fluids with enhanced Viscoleastic properties*
18:00 – 18:20	M. Ehresmann, G. Herdrich	*Overview on ferrofluid space application activities*
18:20	***Poster Session***	

Thursday, September 26th

approx. 08:30 **Mountain and Alternative Tour**

approx. 13:30 **Mountain Talks**

The speakers will be announced in the final program within the book of abstracts.

17:00 **Presentations of the awardees of the "Promotionspreis des Ferrofluidverein Deutschland e.V."**

19:00 ***Workshop dinner***

Friday, September 27th

8:40	**Session 3**	
8:40 – 9:00	L. Fischer, A. M. Menzel	*Maximized magnetoelastic effects through internal structuring of magnetic elastomers*
9:00 – 9:20	P. Gebhart, T. Wallmersperger	*Variational-based modeling of soft and hard magneto-active polymers across scales*
9:20 – 9:40	K.A. Kalina, P. Gebhardt, J. Brummund, W. Sun, M. Kästner	*Neural networks meet magneto-mechanics: A framework for automated model generation*
9:40 – 10:00	D. Romeis, M. Roghani, M. Saphiannikova	*Towards an effective material model for magneto-active elastomers*
10:00	***Coffee break & Posters***	
10:30	**Session 4**	
10:30 – 10:50	H. Nádasi, A. Jarosik, A. Eremin, P. M. Rupnik, A. Mertelj, N. Sebastián, D. Lisjak, M. Küster, F. Ludwig	*Nonlinear optical and magneto-electric effect in multiferroic LC hybrids*
10:50 – 11:10	G. Richwien, B. Rhein, J. Kopp, H. Nádasi, A. Eremin, J. Landers, A. M. Schmidt	*The role of shape anisotropy of hematite nanodopants in ferronematic liquids*
11:10 – 11:30	M. A. Raphael, Y. Martinez, M. Effertz, J. Landers, S. Salamon, H. Wende, A. M. Schmidt	*Synthesis and characterization of multifunctional Pt@[CoFe2O4]n hybrid nanoparticles*
11:30 – 11:50	J. Landers, M. A. Raphael, S. Salamon, H. Wende, A. M. Schmidt	*Tunable magnetic behavior in Pt@[CoFe2O4]n hybrid nanoparticles*
11:50 – 12:10	M. Weißpflog, N. Nguyen, N. Sobania, B. Hankiewicz	*Non-Stoichiometric Cobalt Ferrite Nanoparticles by Green Hydrothermal Synthesis and their Potential for Hyperthermia Applications*
12:15	***Closing***	

Abstracts (Each oral presentation should also be supported by a poster!)

20th FERROFLUIDWORKSHOP

Abstracts

FOR 5599 – From production processes of structured magnetic elastomers to their macroscopic material behavior

G. K. Auernhammer[1], M. Kästner[2], S. Odenbach[2], B. Watzka[3], A. M. Menzel[3]

[1] *Leibniz Institute of Polymer Research Dresden, Dresden, Germany*
[2] *TU Dresden, Dresden, Germany*
[3] *Otto von Guericke University Magdeburg, Magdeburg, Germany*

Background

In March 2024, the German Research Foundation (Deutsche Forschungsgemeinschaft, DFG) decided to establish the new Research Unit FOR 5599 "From production processes of structured magnetic elastomers to their macroscopic material behavior" [1]. We hereby inform our scientific community (you) about this decision and our plans, also in view of evolution towards new collaborative programs.

Scope

In our community, magnetic elastomers have been investigated over the past few years extensively. Our focus is on magnetizable particles of several to many micrometers in size enclosed by soft elastic carrier matrices. We know that magnetorheological and magnetostrictive effects are observed for these materials. Structuring (spatially arranging) the positioning of the magnetizable particles plays a central role. However, we do not really know yet which structures imply the most pronounced response of the materials and, specifically, how these structures can be generated. Moreover, to put it mildly, there is still room for us to communicate the appeal of our research to a broader public outside our scientific community.

Plan of FOR 5599

To address these points, we combine expertise and methods of five complementary areas. On the microscopic particle scale, we try to understand and work out methods to guide the processes of structure formation. Experiments [2] and theory [3] supplement each other. On the macroscopic scale of the materials, we infer how such microscopic structures affect the overall material properties. This is achieved via scale-bridging simulations [4] and through complementary structural analysis combined with macroscopic measurements on real samples [5]. A major goal of FOR 5599 is to further investigate how such information and results are best communicated to a broader public, particularly outside the scientific community. To this end, didactics and educational research represent a central component of the Research Unit [6]. We analyze how corresponding educational materials are perceived and processed, particularly by high-school students, and how educational materials are improved.

Outreach

In parallel, this plan allows to directly convey our results and fascination for the subject to a central target group outside science, namely pupils. We hope to stimulate in this way aspiration for STEM sciences, noting the importance for the general future development of our society.

Acknowledgments

We acknowledge the upcoming support by the DFG in the framework of the Research Unit FOR 5599.

References

[1] https://gepris.dfg.de/gepris/projekt/511114185?language=en.
[2] https://gepris.dfg.de/gepris/projekt/535769078.
[3] https://gepris.dfg.de/gepris/projekt/535543971.
[4] https://gepris.dfg.de/gepris/projekt/535639916.
[5] https://gepris.dfg.de/gepris/projekt/535746395.
[6] https://gepris.dfg.de/gepris/projekt/535548756.

MAE cantilever-type acceleration sensor with adjustable sensitivity

T. I. Becker, L. Zentner

Mechanics of Compliant Systems Group, Faculty of Mechanical Engineering, Technische Universität Ilmenau, 98684 Ilmenau, Germany

In application involving crashes and falls, an acceleration sensor may experience sudden, short-duration impulsive loads and should withstand them without failure. The ultimate design of an accelerometer is usually chosen so that the sensitivity matches a certain range of accelerations that are expected in a particular application. The use of smart materials, such as magnetoactive elastomers (MAEs), in the design of functional proof elements can enable adjustable sensor sensitivity tailored to specific application requirements. This enhances the measurement accuracy and extends the operating range for different acceleration levels. The underlying effect is that the mechanical properties of MAEs can be controlled in a non-contact manner by applying a magnetic field [1,2,3].
Figure 1 shows a prototype of an acceleration sensor with an MAE functional element in the form of a cantilever, synthesized from silicone filled with 30 vol.% carbonyl iron particles. The MAE cantilever is mounted within the air core of a cylindrical electromagnetic coil, which is designed to be powered by an ordinary laboratory source. When the sensor experiences external periodic or transient excitations, the cantilever vibrates, causing magnetic field distortions that are measured by two Hall effect sensors. Their position and orientation within the air core in the plane of cantilever's bending vibrations are determined based on magnetostatic simulations to maximize the measured field response.
The active magnetic control is achieved by regulating the coil current and has a double sense. The field generated inside the coil is necessary, first, to detect external excitation by magnetizing the MAE cantilever, the vibrations of which cause field distortions. Secondly, the coil field affects the vibration characteristics of the cantilever, thereby adjusting the sensor response to an input excitation.

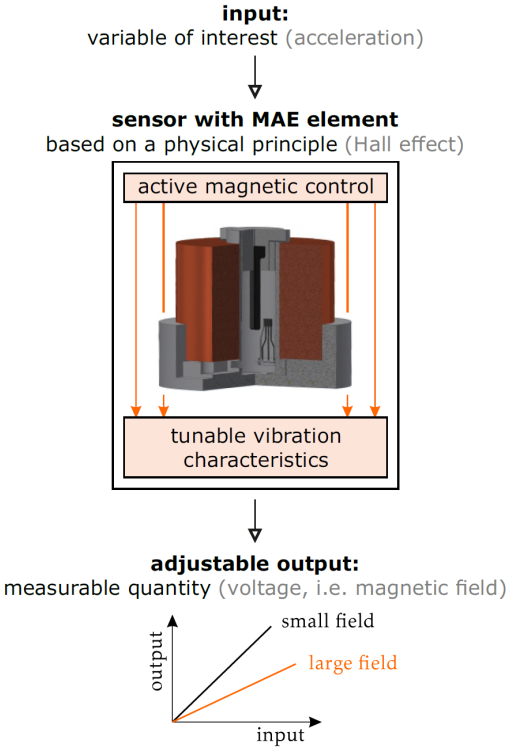

Figure 1. Functioning principle of the MAE cantilever-type acceleration sensor with adjustable sensitivity.

Sensor frequency response

The resonance characteristics of the MAE cantilever-type acceleration sensor are identified by the frequency response to a kinematic harmonic excitation. The sensor outputs a steady-state voltage signal proportional to the difference of horizontal field distortions recorded by the Hall effects sensors. Figure 2 shows the amplitude response as the normalized field difference relative to the undistorted field at the coil center for upward and downward excitation frequency sweeps. The measurements reveal the first bending eigenfrequencies of the MAE functional element, which depend of the current supplied to the coil. Both resonance frequency ranges are narrow and clearly separated from each other without intersection. This ensures a predictable sensor response and determines frequency

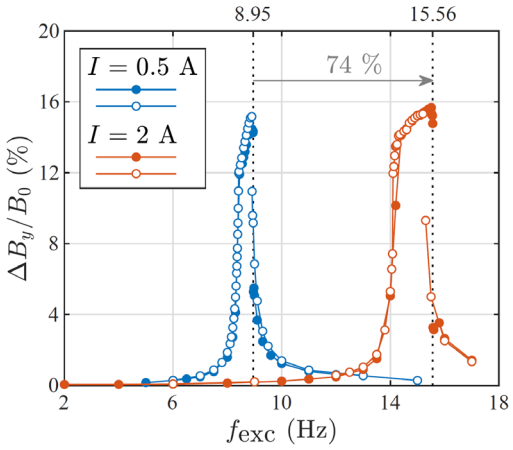

Figure 2. Field distortion response of the sensor for two supplying coil currents: thick and white markers are values obtained during step increase and decrease of the excitation frequency, respectively.

ranges to adjust the sensor operating sensitivity.

Sensor shock response

The sensor response to a mechanical shock is analyzed in the time domain, focusing on the maximum acceleration and field change sensed immediately after a shock load. An individual shock is applied by hand pushing the sensor until it collides with the slide border, in the direction aligned with the MAE cantilever deflection axis (Figure 3). To sufficiently characterize the shock event, both the peak acceleration value a_s and the shock duration t_s

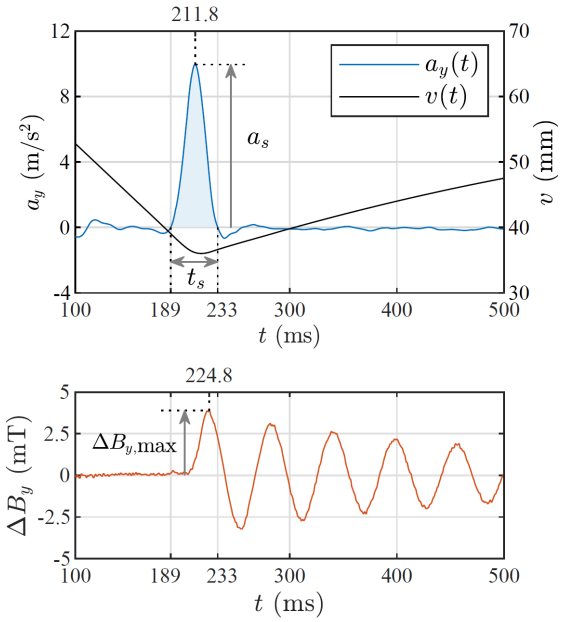

Figure 3. Measurement of an individual shock event for a coil current I = 2.5 A: (top) time sequence of a shock event; (bottom) horizontal field difference recorded by two Hall sensors.

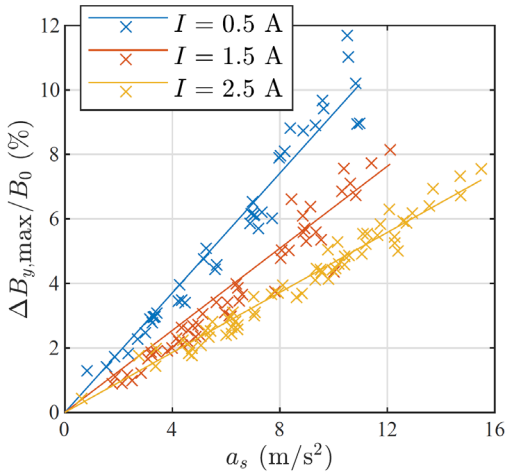

Figure 4. Sensor sensitivity to shock acceleration for different coil currents: experimental data (markers) and linear fit through the origin (solid lines).

are equally relevant, since shocks of different forms and durations may have different impacts on an object.

Figure 4 shows the normalized maximum field change determined for various peak accelerations impacting on the sensor, when the coil is supplied by three different currents. Each group of experimental data is fitted with a line passing through the origin, indicating the proportionality between the input and output. The slopes of these lines give the sensitivity for each coil current.

Acknowledgments

The work is supported by the Deutsche Forschungsgemeinschaft under project BE-6553/2-1.

References

[1] T.I. Becker, O.V. Stolbov, A.M. Biller, D.Yu. Borin, O.S. Stolbova, K. Zimmermann, Yu. L. Raikher. Shape-programmable cantilever made of a magnetoactive elastomer of mixed content. Smart Materials and Structures 31 (2022) 105021 (14pp).

[2] T.I. Becker, Yu.L. Raikher, O.V. Stolbov, V. Böhm, and K. Zimmermann. Magnetoactive elastomers for magnetically tunable vibrating sensor systems. Physical Sciences Reviews 7(10) (2022) pp. 1063-1090.

[3] M. Reiche, T.I. Becker, G.V. Stepanov, K. Zimmermann. A multipole magnetoactive elastomer for vibration-driven locomotion. Soft Robotics 10(4) (2023) 770-784.

Particle diffusion in a ferrogranulate layer induced by competing interactions

O. Bilous[1], Kirill A. Okrugin[1], A. Lakkis[2], P.A. Sanchez[1], R. Richter[2] and S.S. Kantorovich[1]

[1]University of Vienna, Kolingasse 14-16, Vienna, 1090 (Austria)
[2]Experimentalphysik V, Universtät Bayreuth, 95440 Bayreuth (Germany)

Introduction

Ferrogranulate is a granular composite made up of glass and magnetised steel particles that interact through contact forces and external fields, leading to phenomena such as caging, anomalous diffusion, and phase transitions. Advancement in ferrogranulate study dates back to the late 1990s, with numerous researchers such as Duran, Aranson, and Ottino conducting a combined experimental and simulation study on granular materials.

Several years later, quite small charged granules were replaced by millimiter-sized magnetised beads in the experiments by Blair and Kudrolli [1]. Quenching the system from the gas phase into the mixed phase, the authors found loose networks that with time collapsed into compact regions.

In contrast, for a deep quench, the difference in mobility of glass (fast phase) and slowed down by magnetic interactions steel beads, which led to the formation of transient networks that coarsen over time to more compact clusters [2].

Figure 1. Ferrogranulate time evolution (from the left to right) after quenching. Experiment (above). Simulations (below). The details can be found in [2].

This scenario resembles viscoelastic phase separation (VPS) [3] that arises from the different dynamics of the components of the ferrogranulate.

We investigate this dynamic using both theoretical [4, 5] and experimental [4, 6] methods. This investigation was conducted with and without a magnetic field applied perpendicular to the layer. We focus on the ferrogranulate system, which contains different total area fractions and changes the concentration of magnetic and steel beads.

Methods

In the theoretical part of our study, we investigate Brownian motion in a quasi-two-dimensional ferrogranulate system through molecular dynamics simulations. The system is made up of millimetre-sized magnetic and glass spheres with diameters of $\sigma_m = 3$ and $\sigma_g = 4$, respectively. These spheres are modeled using a combination of Stockmayer and Weeks-Chandler-Andersen potentials, with thermal fluctuations simulating the shaking amplitude. Each sphere is characterised by a magnetic point dipole at its centre. Our preliminary findings suggest that the magnetic susceptibility of the steel spheres can be accurately reproduced by introducing an additional central attraction, scaled by ε, between the steel spheres. The simulations are conducted using the ESPResSO 4.1.4 package.

Numerical results

In particular, we calculate the mean number of nearest neighbours of each magnetic particle, and plot them as functions of time Fig. 2. From this analysis we observe that over time, the system reaches a diffusion regime, allowing us to calculate the diffusion coefficient by analysing the mean square displacement (MSD).

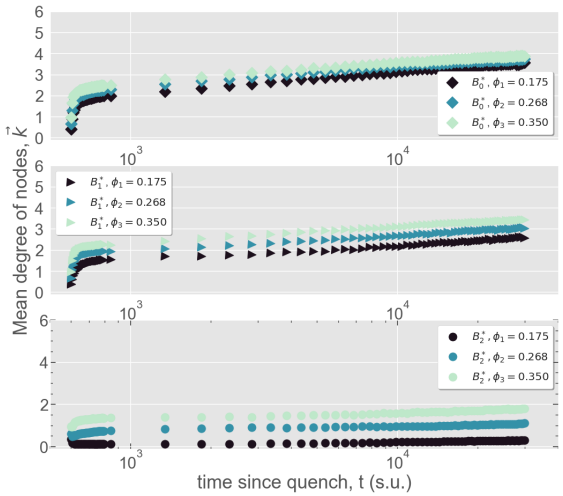

Figure 2. Mean degree of a node versus simulation time for different applied magnetic fields $|B^*_{z0}|$=0.0; $|B^*_{z1}|$=0.5; $|B^*_{z2}|$=1.0 (different the symbols mark) and three different total area fractions (different colour) $\varphi_n=\varphi_m+\varphi_g$, where φ_m – magnetic particles and φ_g – glass particles; φ_1 = 0.1+0.075; φ_2 = 0.153+0.115, φ_3 = 0.2+0.15 in simulation units.

Our findings show that an increase in total concentration slows down cluster dynamics and increases the probability of larger clusters, which in turn hinders the system's response to the magnetic field. At low applied field values, the calculations suggest the presence of a bistable region at high concentrations, where droplet precursors form.

By MSD analysis (Fig. 3) for four different particle configurations, including magnetic particles in clusters, singular magnetic particles, total magnetic particles, and glass particles, we uncover distinct regimes of Brownian dynamics.

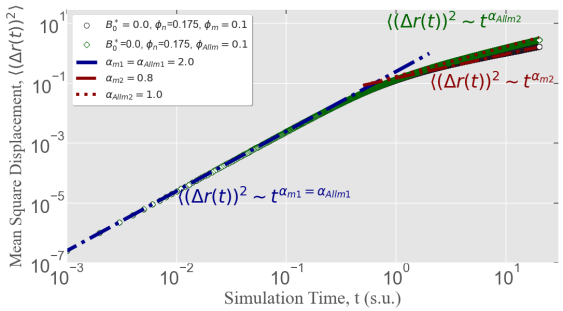

Figure 3. MSD for φ_1 = (0.1+0.075) and $|B^*_0|$ = 0.0. The colour of the line corresponds to different diffusion regimes.

These regimes include ballistic motion, superdiffusion, and a transition to subdiffusion or continued superdiffusion, depending on the type of particles and their configuration. Normal diffusion is achieved when both the external magnetic field strength and area fraction are maximised, except for magnetic particles that are clustered together.

Our investigation uncovers complex diffusion behaviour across various area fractions of magnetic and glass beads and three external magnetic field strengths (B^*_{z0} = 0.0, B^*_{z1} = 0.5, B^*_{z2}=1.0) perpendicular to the monolayer, leading to transitions between different Brownian dynamics regimes.

We also observe a complex interplay between the repulsion of magnetised beads aligned with the applied field and the dipolar forces that tend to orient the magnetisation within the layer plane, leading to aggregation. This study offers valuable insights into the fundamental mechanisms governing diffusion in ferrogranulate layers, with implications for various scientific and technological applications.

Acknowledgements
The authors acknowledge financial support for the German-Austrian project "Coarsening dynamics of ferromagnetic granular networks: experiment and simulation" through Ri 1054/7-1 and I5160 FWF.

References

[1] D.L. Blair and A. Kudrolli, Phys. Rev. E 67 (2003) 021302.

[2] A. Kögel, P. Sanchez, R. Maretzki, T. Dumont, E. S. Pyanzina, S. S. Kantorovich, and R. Richter. Soft Matter, 14 (2018) 1001.

[3] H. Tanaka, J. Phys: Condens. Matter 12 (2000) R207.

[4] M. Biersack, A. Lakkis, R. Richter, O. Bilous, P.A. Sanchez, S.S. Kantorovich, Phys. Rev. E. 108 (2023) 054905.

[5] O. Bilous, M. Biersack, A. Lakkis, R. Richter, and S. Kantorovich, Journal of Magnetism and Magnetic Materials, 589 (2024) 171627.

[6] A. Lakkis, M. Biersack, O. Bilous, S. Kantorovich, R. Richter, J. Magn. Magn. Mater. 589 (2024) 171620.

Experiments towards understanding the failure mechanism of magnetic microparticle structures in quasi-static shear

D. Borin, Y. Jiang, S. Odenbach

Technische Universität Dresden, 01069 Dresden, Germany

Magnetorheological (MR) fluids are suspensions of micron-sized magnetic particles in a carrier liquid medium. They are named due to significant changes in rheological behavior depending on the strength of the applied external magnetic field. For example, the change in yield stress can reach several orders of magnitude. Despite the active research of MR fluids for more than half a century, there are still a number of important, but not clarified from the point of view of basic physics, aspects related to the macroscopic response of these materials to external influences. One of these is the clarification of the mechanism of breaking of the MR fluid structured in the magnetic field under shear stresses and correspondingly related quasi-static elastic properties of the material. A number of previously published theoretical models and computer simulations are known on this subject, considering both aggregates of magnetic microparticles in the form of simple linear chains, cylinders, or ellipsoids, and in the form of branched labyrinth structures [1-3]. The expected response under quasi-static shear of a structured MR fluid is a monotonic stress growth, from the slope of which the regions of pre yield and post yield behaviour are determined [2]. It is as well reported that under certain conditions, the models demonstrate a non-monotonic dependence of shear stress on macroscopic shear [1, 3]. As it is pointed out in [3], the state of the system with a decreasing dependence of stress on shear strain is mechanically absolutely unstable, since the smallest internal fluctuations of deformation should grow rather than dissipate. Hence the difficulties in detecting such a state in experimental studies. In fact, almost all experimental studies known to us show a monotonic dependence of shear stress on strain/time. In single cases (see e.g. Fig. 3a in [4]), however, overshooting can also be observed in the plots of the presented measurement results, but no attention has been given to it by investigators. In such a context, our work is devoted to attempts to find experimental conditions in which a non-monotonic dependence of the shear stress at quasi-static shear stress is observed for a structured MR fluid of the simplest possible and known composition. In this case, we vary such parameters as the concentration of magnetic particles, the size of the working gap between the static and shear plates, and the strength of the external magnetic field. We also focus on the material and surface roughness of the working plates. In addition to the fundamental importance, the expected results are essential from an applied point of view for the choice of MR fluid and operating conditions for devices using magnetic control of the static yield stress. This is particularly the case for MR disc brakes or MR dampers with MR valve operating in a shear mode. Preliminary results of our research will be presented at the workshop.

Acknowledgments

The financial support by German Federal Ministry of Education and Research within the KMU-innovativ - collaborative project "COGNAC" under contract number 13GW0632D is gratefully acknowledged.

References

[1] Bossis et al 1997, J. Rheol. 41, 687
[2] Gandhi et al 2005, J. Int. Mat. Sys. Str. 16, 237
[3] Zubarev et al 2020 Eur. Ph. J. ST 229, 2967–79
[4] Zhang et al 2008, Kr.-Astr. Rheol. J. 20, 45-50.

Increase of MPS signal by isotropic aggregates of magnetic nanoparticles

D. Eberbeck[1], F. Wiekhorst[1]

[1] *Physikalisch-Technische Bundesanstalt, Berlin, Germany*

In this study, the effect of the aggregation of magnetic nanoparticles (MNP) as tracers for Magnetic Particle Imaging (MPI) within different matrices was investigated. Embedding of MNP in matrices often immobilizes the MNP which decreases the resolution of MPI and correspondingly the amplitudes of the Magnetic Particle Spectroscopy (MPS) signal, as it is shown exemplarily for Resovist® after immobilization of the MNP by freeze drying in a mannitol matrix (Fig. 1).
Chaining of MNP by immobilisation of MNP in matrices under an external field usually enhances the susceptibility but isotropic aggregates in most cases decrease the MPS-signal because of the competing character of dipole-dipole interaction in disordered systems [1], except for very small MNP with diameters below 10 nm.
Here we observed for some commercial available synomag® (micromod Partikeltechnologie GmbH) samples the opposite. In a wide range of higher harmonics the signal for citrate coated ("C") synomag SynC30a increases after freeze drying within a mannitol matrix (Fig. 1) while it decreases for the non-coated SynP50 ("P"-plain surface) (Fig. 1) and the samples with the larger sizes and related larger moments (Table 1).
In order to elucidate this behaviour, we investigated the structure of possible aggregates within the mannitol matrix. To this end, the Small Angle X-ray Scattering (SAXS) intensities of the MNP dispersed in mannitol solution was measured at room temperature and in frozen state at 253 K with a SAXSpace measurement device (Anton Paar, Austria). After subtraction of the background and desmearing the pair distance distribution, PDDF, was calculated by Fourier transformation.
The results of the two sytems with the extrem values of the magnetic moment show strong differences in the structure of aggregates. While the MNP of SynP50 produce large aggregates ($\approx 250\,\mathrm{nm}$), those of SynC30a measure about $180\,\mathrm{nm}$.

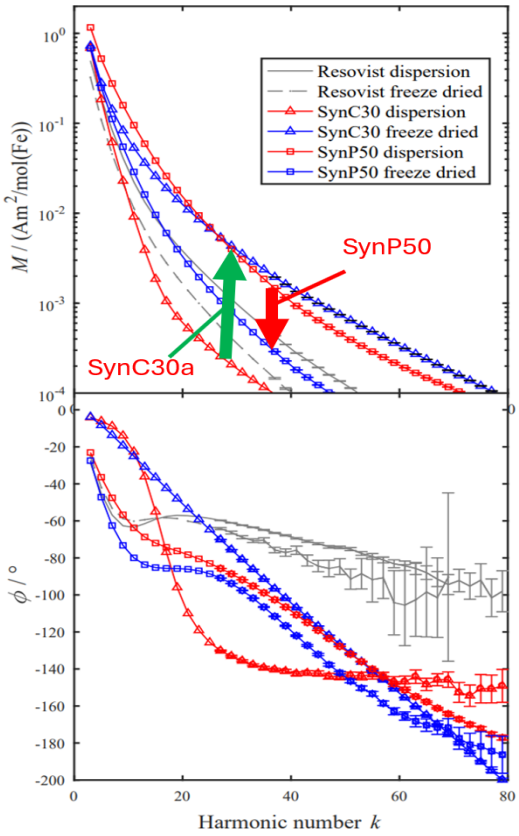

Figure 1: MPS-data, harmonics of magnetisation and phase lag, ϕ, for 2 synomag systems and the established MPI-tracer Resovist® before (red) and after freeze drying (blue). The arrows emphasize the signal change following to freeze drying.

Furthermore, the low absolute value of the PDDF of SynC30 is evidence of a lower packing fraction of $\phi_{c,A} = 6\%$ in comparison to $\phi_{c,A} = 24\%$ for aggregates of SynP50 (Table 1).
This conclusion was supported by calculation of the scattering curves and PDDF for aggregates modelled with "Random aggregation" (RA) and "Diffusion Limited Aggregation" procedures [2]. While the compact aggregates of SynP50 can't be described by the loosely packed DLA, the data of SynC30 could be described by DLA quite good (Fig. 2).

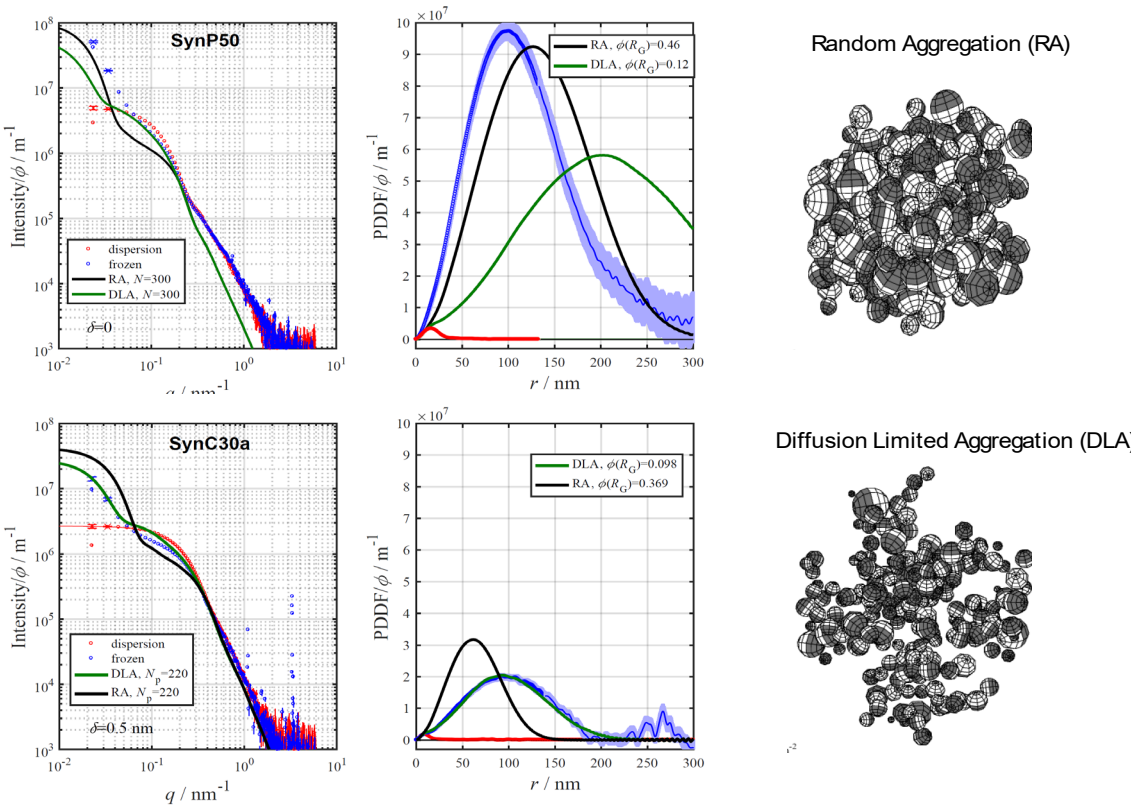

Figure 2: SAXS-Intensities after background correction (left column) and normalized with respect to the magnetite volume fraction, ϕ, and pair distribution function (PDDF), calculated from desmeared intensities (center column), measured (points) at ambient temperature ("dispersion") and 253 K ("frozen"). Crosses: data, correction of beam stop shadowing. The lighter colored band around PDDF represents its uncertainty range. Model curves were calculated for RA- and DLA-aggregates (right column) with the structure parameters of the constituting MNP-cores, coating layer thickness δ, indicated number of MNP per aggregate, N, resulting in the indicated mean volume fraction of MNP, $\phi(R_G)$, within the Guinier Radius, R_G, of the aggregates.

Table 1: Mean magnetic moment of the MNP-cores, μ, relative change of MPS-harmonics M_{21} and volume fraction of MNP-cores within aggregates, $\phi_{c,A}$, estimated from SAXS-data. The iron concentrations of the samples were (10…20) mmol/L.

MNP	μ aAm^2	ΔM_{21}	$\phi_{c,A}$
SynC30a	0.6(1)	182%	0.06(2)
SynC30b	1.1(1)	64%	0.10(3)
SynC30c	2.1(2)	-116%	0.23(3)
SynC50	4.6(5)	-184%	0.16(5)
SynP50	5.0(5)	-130%	0.24(5)

Interpretation: The degree of competing character of the dipole-dipole interaction is lower in DLA-like aggregates due to reduced number of nearest neighbours. Also, the smaller moments seem to support the ease of locally parallel coupling of neighboring moments and its reorientation along the external fields. This might lead to a more collective behaviour of the monments. The qualitatively different, strongly linear decay of $\phi(k)$ for SynC30a in freeze dried state (Fig. 1) hints at that hypothesis.

It seems to be likely that a fine tuning of particle moment and coating can bear a magnetic readout system, very sensitive for changes of the matrix which affects the MNP aggregate structure, like for example early changes of extracellular matrix before a desease.

References

[1] E. I. Wisotzki, D. Eberbeck, H. Kratz, and S. G. Mayr, Soft Matter **12**, 3908 (2016).

Overview on ferrofluid space application activities

M. Ehresmann[1], G. Herdrich[2]

[1] *Institute of Space Systems, University of Stuttgart, ehresmann@irs.uni-stuttgart.de*
[2] *Institute of Space Systems, University of Stuttgart, herdrich@irs.uni-stuttgart.de*

In space applications, mechanical devices introduce significant liabilities, including heightened development risks and potential mission failures. The inherent wear of tribological surfaces demands precise mechanism design, extensive lifetime testing, and the use of expensive, high-performance materials to ensure the reliability of components that must endure long-term operation or extended dormancy in the harsh space environment.
Ferrofluids are a key component to convert a mechanical component into a non-tribological (i. e. low wear and tear) device.
To assess ferrofluid viability to address the challenge of mechanical space components, the Institute of Space Systems has conducted several projects aimed at validating the use of ferrofluids in space environments. Successful microgravity tests have demonstrated a range of ferrofluid applications, including ferrofluid droplet dynamics on the ISS, reaction wheel operation, electrical current switching using magnetic liquid metals, thermal load regulation, and the pumping of non-magnetic liquids via a fully fluidic system driven by a ferrofluid-suspended piston.
Additional applications that have been studied in prototype forms are fully fluidic reaction wheels, bearings, sealings, electro-permanent magnets, magnetorquers, various gearing applications and axle feedthroughs.
This exploration of ferrofluid for space applications began in 2016 with the DLR Space Agency's Überflieger competition, which invited student teams to propose experiments for 30 days of operation on the International Space Station (ISS). One of the winning proposals PAPELL (Pump Application using Pulsed Electromagnets for Liquid Relocation) [1], allowed for the manipulation of ferrofluid using commercial electromagnets during a 100-day ISS mission from 2018 to 2019. In the microgravity environment, the experiment successfully demonstrated ferrofluid droplet generation, movement, splitting, and merging, fulfilling the conditions for digital microfluidic circuits. This achievement opens the door to a wide range of potential applications.
A subsequent project, FerrAC (Ferrofluid Attitude Control), focused on utilizing ferrofluid to develop a non-mechanical attitude control system for spaceflight [2]. Typically, mechanical systems such as reaction wheels are employed for this purpose, where the exchange of angular momentum between a fast-rotating flywheel and the host satellite enables adjustments to the satellite's pointing attitude.
Two primary non-mechanical concepts have been investigated. The first involves distributing angular momentum through a pipe system within the satellite, requiring a non-mechanical pump to drive the working fluid. The second concept, analogous to a reaction wheel, uses a liquid wheel, where a containment partially filled with ferrofluid is subjected to a rotating magnetic field to achieve attitude control capabilities.
Two variants of the pump-in-loop concept were flown in 2024 aboard a REXUS sounding rocket as part of the FerrAS (Ferrofluid Application Study) student project. The displacement pump variant achieved a mass flow of up to 25 ml/min [3]. In this system, three permanent magnets, coated with EFH-1 ferrofluid, serve as both bearings and seals to effectively drive the working liquid. Electromagnetic fields generated by solenoids define the movement of the magnets.
The second variant, the linear pump, operates without any solid moving parts. Ferrofluid is magnetically pinned along the working fluid channel by permanent magnets. A series of electromagnets generates a magnetic wave that shapes the ferrofluid, allowing it to drive the working liquid. This pump achieved a flow rate of 5 ml/min.

The prototype for the fully fluidic reaction wheel did not achieve sufficient RPM to be considered an effective reaction control actuator. Consequently, the system was upgraded to a solid rotor or flywheel suspended on permanent magnets wetted with ferrofluid to still achieve a non-tribological system [4]. This configuration allows for the creation of a low-friction bearing, while direct magnetic coupling with the permanent magnets enables the system to operate within the desired range of over 1,000 RPM. This system was initially conceptualized and prototyped during the FerrAC project.

Experiment operation of this reaction wheel was made possible through the Überflieger 2 program, where a student team was given approximately one month on the ISS in 2023 to conduct their proposed experiment, FARGO (Ferrofluid Application Research Goes Orbital) [5].

Additionally, the FARGO experiment container housed two other technology demonstration experiments.

The first was a thermal switch, which utilized the differing thermal conductivities of EFH-1 ferrofluid and air to create a switchable heat conduction element. This was achieved by adjusting the position of the ferrofluid using a magnetic field.

The second experiment involved an electric switch using a magnetizable variant of the room-temperature liquid metal alloy Galinstan (composed of gallium, indium, and tin) and an insulating oil. By adding micrometer-sized iron particles to the alloy, paramagnetic behavior similar to conventional ferrofluid was induced [6]. However, at the current state of the art, magnetizable Galinstan is not considered long-term stable.

Switching is realized using magnetic fields to allow the magnetic Galinstan to make and break the electrical contact.

Both switch types employed electro-permanent magnets, creating a highly efficient system that required energy input only for switching states. Several thousand switching cycles for both switch types were successfully performed with this setup on the ISS [7].

Currently, efforts are underway to advance the displacement pump and electrical switch technologies as part of the REXUS sounding rocket experiment, FINIX (Ferrofluid Implementations for Next-generatIon Exploration) [8]. Additionally, prototype development is ongoing for potential applications of ferrofluid in bearings, sealing mechanisms, optical systems, and gear assemblies.

These ongoing advancements demonstrate the versatility and potential of ferrofluids in space applications, addressing critical challenges associated with mechanical systems in harsh environments. By leveraging their unique properties, such as low wear, fluidic motion control, and magnetic manipulation, ferrofluids offer promising alternatives to traditional tribological components. As development continues, ferrofluids are likely to play a pivotal role in the next generation of spacecraft systems, contributing to more efficient, reliable, and cost-effective space missions.

Acknowledgments

This work was funded by the Federal Ministry for Economic Affairs and Energy based on a resolution by the German Bundestag. grant no. 50RK1973 (FerrAC), the Überflieger 1 (PAPELL) and Überflieger 2 (FARGO)student team competition as well as the REXUSBEXUS (FerrAS & FINIX) programme by DLR, ESA and SNSC.

References

[1] M. Ehresmann, et al.: Experiment Results and post-flight Analysis of the ISS Student Experiment PAPELL, 70th IAC; 2019

[2] M. Ehresmann et al.: Final Results of the novel ACS development project FerrAC, 74th IAC,2023

[3] B. Karahan et al.: Preliminary Results of Novel Ferrofluidic Systems Tested on a REXUS Sounding Rocket, ESA PAC Symposium, 2024

[4] S. Zajonz et al.: Development of a Ferrofluid-Based Attitude Control Actuator for Verification on the ISS, Aerotecnica Missili & Spazio 103(3), 2024

[5] S. Sütterlin et al.: Fargo: validation of space-relevant ferrofluid applications on the ISS, CEAS Space Journal, 2024

[6] L. Hu et al.:Magnetic liquid metals manipulated in the three-dimensional free space, ACS Appl. Mater. Interfaces 11(8), 8685–8692, 2019

[7] J. Dietrich et al.: Scientific Results of FARGO -A Verification of Novel Ferrofluid Systems on the ISS, 74th IAC, 2023

[8] FINIX project page, https://www.ksat-stuttgart.de/de/finix/ , accessed 10.09.2024

Maximized magnetoelastic effects through internal structuring of magnetic elastomers

L. Fischer, A. M. Menzel

Institut für Physik, Otto-von-Guericke-Universität Magdeburg, Universitätsplatz 2, 39106 Magdeburg, Germany

Overview

One prominent feature of magnetic gels and elastomers is their magnetostrictive behavior. The application of homogeneous external magnetic fields stimulates overall macroscopic deformations [1,2]. Additionally, these materials feature magnetorheological effects. That is, changes in their rheological properties are induced by external magnetic fields [3].

Motivation

Magnetic gels and elastomers are hybrid materials that consist of a soft, usually polymeric elastic matrix that encloses magnetic or magnetizable inclusions of submicrometer to submillimeter size. On the one hand, their magnetostrictive response makes them promising candidates for application as soft actuators or artificial muscles. On the other hand, their magnetorheological properties qualify them for application as adaptive dampers. Generally, from these perspectives, a maximized response to the applied external magnetic field is beneficial.

We have developed a scale-bridging approach that we apply to theoretically determine the magnetoelastic response of example systems of magnetic elastomers. On its basis, we can directly calculate from the microscopic scale of the particulate inclusions and their spatial arrangement the resulting macroscopic mechanical material response upon magnetization [4]. Specifically and in contrast to several other approaches, we explicitly include in our theory the finite size of the systems. Then, the displacements of the boundaries represent the overall deformation of the system as it is observed from outside.

Theoretical description

For simplicity, we first study systems of overall spherical shape. This allows us to develop an analytical approach, based on linear elasticity theory. Through these means, we calculate the overall deformation of the spherical system starting from the forces that the microscopic inclusions transmit to the soft elastic carrier matrix [4,5]. Hereby, we assume the elastic matrix to be fully homogeneous and isotropic. We focus on two types of overall deformation induced by magnetization of the inclusions. These are overall changes in volume as well as relative elongation or contraction along the direction of the magnetic field [6,7]. We assume all magnetizable inclusions to be identical and point-like, describing their magnetic interactions in terms of magnetic dipoles. Previous works include aspects of polydisperse systems [8], induced torsional deformations through appropriate positioning of the inclusions [9], as well as higher-order modes of deformation [10].

Second, we turn to systems of overall cubical shape. In this context, we analyze magnetorheological effects resulting from prescribed spatial positioning of the magnetizable inclusions in the elastic matrix.

For both scenarios, we determine the specific internal structures that maximize the resulting effects. That is, we now determine for a specific mode of deformation or for the requested type of magnetorheological effect the arrangement of magnetizable inclusions that leads to the maximum performance [6]. Optimization is achieved by numerically evaluating corresponding scale-bridging analytical formulae and iteratively improving the arrangement of magnetizable inclusions following an adjusted numerical scheme of simulated annealing [11].

Results

For maximized elongation along the external magnetic field direction, we find an optimized structure that resembles a rotated simple cubic lattice. Contrarily, for maximized contraction, hexagonal chain-like arrangements are close to optimal, with chains oriented along the field direction. For maximized shrinkage (decrease in volume), the optimized structures approximately feature chains along the field direction, with irregular arrangements of the chains. Instead, maximized increase in volume is achieved by structures close to hexagonal layers of inclusions, with the layer normal oriented along the field direction. For all these effects, we additionally study the influence of the number of magnetizable inclusions and of the compressibility of the elastic matrix.

Concerning optimized magnetorheological effects, we consider the increase in elastic moduli with respect to uniaxial elongation or simple shear. For uniaxial elongation, the optimized arrangements are similar to face-centered cubic structures. Conversely, for shear deformations, they resemble hexagonal layers, with one axis of the layers parallel to the field direction.

Conclusions

In summary, we present a route towards magnetic gels and elastomers that feature optimized internal arrangements of magnetizable inclusions, depending on the task that they are intended for. We find that, in general, the resulting optimized structures are not completely regular (lattice-type) arrangements. Besides, they depend on the number of inclusions as well as the properties of the employed elastic matrix. We are optimistic that, in the future, such optimal internal structures of the materials can be realized by modern techniques of fabrication, such as 3D printing. We wish to support their application by providing tools of analysis to optimize the material design.

Acknowledgments

We thank the German Research Foundation (DFG) for support through the Heisenberg grant no. ME 3571/4-1 and through the Research Unit FOR 5599, grant nos. ME 3571/10-1 and ME 3571/11-1.

References

[1] A. M. Menzel, Phys. Rep. **554**, 1 (2015).
[2] A. M. Menzel, H. Löwen, Phys. Sci. Rev. **7**, 1529 (2022).
[3] S. Odenbach, Arch. Appl. Mech. **86**, 269 (2016).
[4] L. Fischer, A. M. Menzel, J. Chem. Phys. 151, 114906 (2019).
[5] L. J. Walpole, Proc. R. Soc. London A **458**, 705 (2002).
[6] L. Fischer, A. M. Menzel, PNAS Nexus (accepted).
[7] L. Fischer, A. M. Menzel, arXiv preprint arXiv:2407.09291.
[8] L. Fischer, A. M. Menzel, Smart Mater. Struct. **30**, 014003 (2021).
[9] L. Fischer, A. M. Menzel, Phys. Rev. Research **2**, 023383 (2020).
[10] L. Fischer, A. M. Menzel, J. Magn. Magn. Mater. **591**, 171695 (2024).
[11] S. Kirkpatrick, C. D. Gelatt, M. P. Vecchi, Science **220**, 671 (1983).

Variational-based modeling of soft and hard magneto-active polymers across scales

Philipp Gebhart, Thomas Wallmersperger

Institute of Solid Mechanics, Technische Universität Dresden, 01062 Dresden, Germany

In recent years there has been an increasing interest in the theoretical and experimental study of field responsive, functional composite materials. Magneto-active polymers (MAPs) are a special class of field responsive solids that comprise of a polymeric matrix with dispersed micro-sized magnetizable particles. As a result of this microstructural composition, these materials deform and alter their material characteristics under the influence of magnetic fields. Based on the magnetic properties of the underlying ferromagnetic filler particles, MAP composites can be classified into two categories: (i) soft and (ii) hard MAPs. Soft MAPs comprising magnetically soft particles, e.g. carbonyl iron, exhibit negligible hysteresis loss and demagnetize completely after the removal of the external magnetic field which in consequence leads to reversible deformation mechanisms. In contrast, NdFeB particle-filled hard MAPs exhibit distinct nonlinear, dissipative material behavior, such as the characteristic magnetic and "butterfly" field-induced strain hysteresis. These properties in combination with the tunability of specific characteristics through the fabrication process make soft and hard MAPs attractive options for various engineering applications.

In the present work, we present a comprehensive microstructural guided modeling framework for hard MAPs including the response of the soft MAPs as a limiting case. We outline ingredients of the constitutive theory based on the framework of generalized standard materials, that necessitates suitable definitions of (i) the total energy density function and (ii) the dissipation potential. Key idea of the constitutive approach is an additive split of the material part of the total energy density function into three contributions associated with (i) an elastic ground stress, (ii) the magnetization and (iii) a magnetically induced mechanical stress, respectively [1, 2]. We propose suitable constitutive functions in an energy-based setting that allow to accurately capture the highly nonlinear material behavior of soft and hard MAPs with stochastic microstructures. Subsequently, the two constitutive functions are embedded in an incremental minimization principle that is supplemented by a conforming finite element method. Furthermore, we discuss polyconvexity of the constitutive model which implies quasiconvexity and rank-one convexity and thus ensures material stability.

The performance of the developed variational-based modeling framework is demonstrated by solving some application-oriented boundary value problems. The main emphasis of the numerical studies lies on the investigation of the magnetostrictive effect of hard MAPs at the macroscale level as well as on the in depth analysis of pre-magnetized beam structures undergoing large deformations.

References

[1] P. Gebhart and T. Wallmersperger, A constitutive macroscale model for compressible magneto-active polymers based on computational homogenization data: Part I - Magnetic linear regime, International Journal of Solids and Structures 236 (2022) 111294.

[2] P. Gebhart and T. Wallmersperger, A constitutive macroscale model for compressible magneto-active polymers based on computational homogenization data: Part II - Magnetic nonlinear regime, International Journal of Solids and Structures 258 (2022) 111984.

Ultrasound-based Methods for Imaging Superparamagnetic Iron Oxide Nanoparticles in Biomedical Applications

C. M. Huber[1,3], H. Ermert[2], I. Ullmann[3], M. Vossiek[3], C. Alexiou[2], S. Lyer[1]

[1] *Department of Otorhinolaryngology, Head and Neck Surgery, Section of Experimental Oncology and Nanomedicine (SEON), Professorship for AI-Controlled Nanomaterials (KINAM), Universitätsklinikum Erlangen, Glücksstrasse 10a, Erlangen, 91054, Bavaria, Germany*
[2] *Department of Otorhinolaryngology, Head and Neck Surgery, Section of Experimental Oncology and Nanomedicine (SEON), Universitätsklinikum Erlangen, Glücksstrasse 10a, Erlangen, 91054, Bavaria, Germany*
[3] *Institute of Microwaves and Photonics (LHFT), Friedrich-Alexander-Universität Erlangen-Nürnberg, Cauerstrasse 9, Erlangen, 91058, Bavaria, Germany*

Motivation

Superparamagnetic iron oxide nanoparticles (SPIONs) are utilized in various biomedical applications, such as local chemotherapy with Magnetic Drug Targeting (MDT) [1], local magnetic hyperthermia [2] and imaging sentinel lymph nodes [3]. Conventional methods for imaging SPIONs are for example magnetic resonance imaging (MRI) [4] or magnetic particle imaging (MPI) [5]. However, these methods are expensive and cannot be performed e.g. during Magnetic Drug Targeting. Ultrasound-based methods, such as magnetomotive ultrasound (MMUS) [6, 7], ultrasound elastography [8, 9] or ultrasound-induces cavitation [10] can be used during most biomedical SPION applications and have the potential for real time imaging.

Magnetomotive Ultrasound

MMUS utilizes the magnetic properties of SPIONs to image their distribution. An applied magnetic field exerts the magnetic gradient force [6]

$$F_m = \frac{\chi_S V}{2\mu_0} \nabla(|\mathbf{B}(\mathbf{r},t)|^2), \qquad (1)$$

on the SPIONs. χ_S is the magnetic susceptibility, μ_0 the permeability, V the volume of magnetic core in each SPION and $\mathbf{B}(\mathbf{r},t)$ the magnetic flux density with point $\mathbf{r} = (x,y,z)^T$ and time t. When an alternating magnetic field is applied to tissue interspersed with SPIONs, these particles and the tissue are displaced according to the magnetic field pattern. The displacement of the tissue can be tracked with ultrasound imaging and reconstructed as the area of SPION-distribution. We demonstrated that this method can even be used during Magnetic Drug Targeting [7] (Figure 1).

Ultrasound Elastography

The accumulation of SPIONs can increase the mechanical stiffness in the corresponding are. This stiffness change can be mapped with ultrasound strain elastography. Using ultrasound, two data sets are acquired and compared. One data set is without any mechanical influence, and the other with. The mechanical excitation can be by compression with the ultrasound transducer or by magnetic displacement. It was demonstrated, that this method can image SPION distribution in ultrasound phantoms [9].

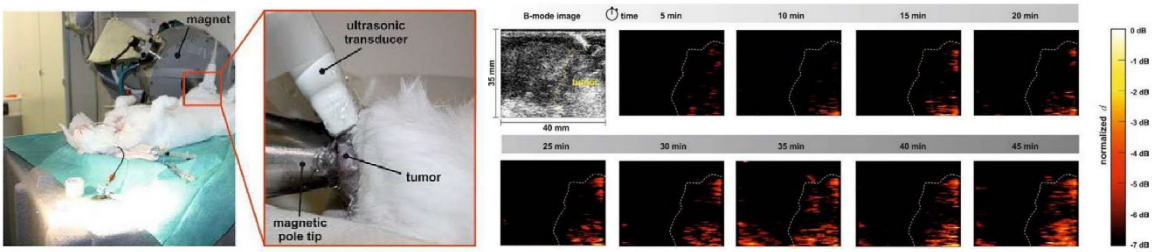

Figure 1: In vivo magnetomotive ultrasound imaging during Magnetic Drug Targeting of a rabbit. The nanoparticle accumulation is monitored over a time frame of 5 minutes to 45 minutes [7].

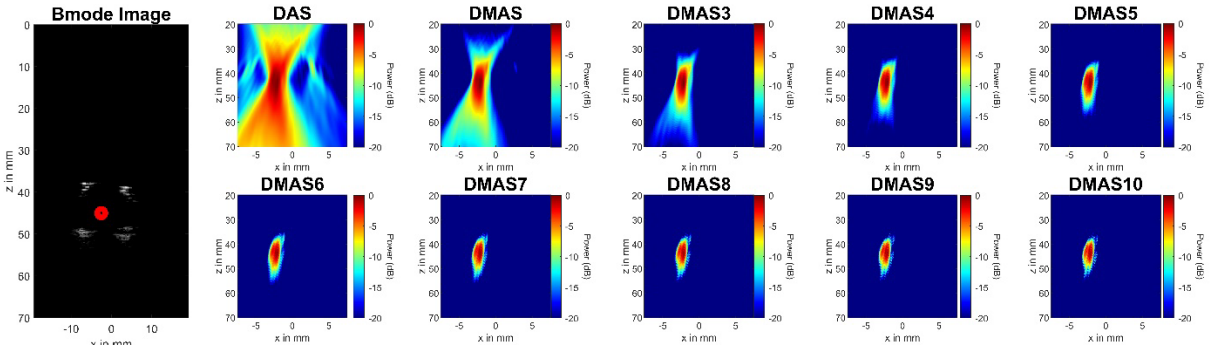

Figure 2: B-mode image of the ultrasound phantom with SPION inclusion (red circle) and corresponding passive cavitation mapping using a higher order Delay Multiply and Sum beamformer.

Ultrasound induced Cavitation

A completely novel ultrasound based imaging method exploits the utilization of focused ultrasound (FUS) induced cavitation on SPIONs. It was shown that certain SPIONs can generate acoustic cavitation when placed in a focused ultrasound wave field [10]. Cavitation is the generation of gas filled microbubbles, which oscillate and eventually implode. These implosions can be detected as acoustical noise signals and used to map the cavitation source area. As the SPIONs serve as cavitation contrast agents, imaging the cavitation source area indirectly maps the SPION distribution. In Figure 2, passive cavitation mapping [11] was used to map the SPION distribution using a higher order Delay Multiply and Sum beamformer.

Conclusion

In our work, we used various ultrasound-based methods for imaging SPIONs. MMUS creates an indirect link for imaging SPIONs utilizing their magnetic properties, while ultrasound elastography relies on the mechanical stiffness of the SPION density in tissue. The newly developed method of passive cavitation mapping uses acoustic properties. In future work, combining these different imaging modalities can create an imaging framework with high precision and various information value.

Acknowledgments

The authors gratefully acknowledge the financial support of the Deutsche Forschungsgemeinschaft (DFG) – project number 452821018, and the Julitta und Richard Müller Stiftung, Munich, Germany.

References

[1] Tietze, R et al. (2013). Efficient drug-delivery using magnetic nanoparticles—biodistribution and therapeutic effects in tumour bearing rabbits. *Nanomedicine: Nanotechnology, Biology and Medicine*, *9*(7), 961-971.

[2] Dutz, S., & Hergt, R. (2013). Magnetic nanoparticle heating and heat transfer on a microscale: Basic principles, realities and physical limitations of hyperthermia for tumour therapy. International Journal of Hyperthermia, 29(8), 790-800.

[3] Evertsson, S. et al. (2017). Combined Magnetomotive ultrasound, PET/CT, and MR imaging of 68Ga-labelled superparamagnetic iron oxide nanoparticles in rat sentinel lymph nodes in vivo. Scientific reports, 7(1), 4824.

[4] Avasthi, A. et al. (2020). Magnetic nano-particles as MRI contrast agents. Surface-modified nanobiomaterials for electrochemical and biomedicine applications, 49-91.

[5] Borgert, J. et al. (2012). Fundamentals and applications of magnetic particle imaging. Journal of cardiovascular computed tomography, 6(3), 149-153.

[6] Oh, J. et al (2006). Detection of magnetic nanoparticles in tissue using magneto-motive ultrasound. Nanotechnology, 17(16), 4183.

[7] Fink, M. et al. (2020). In Vivo study on magnetomotive ultrasound imaging in the framework of nanoparticle based magnetic drug targeting. Current Directions in Biomedical Engineering, 6(3), 543-546.

[8] Fink, M. et al. (2018). Sonographic detection of iron oxide nanoparticles employing shear waves. Current Directions in Biomedical Engineering, 4(1), 457-459.

[9] Huber, C. M. et al. (2024). Magnetically Enhanced Ultrasound Strain Elastography to Visualize Magnetic Nanoparticles.

[10] Huber, C. M. et al. (2022, September). Ultrasound-Mediated Cavitation of Magnetic Nanoparticles for Drug Delivery Applications. In Current Directions in Biomedical Engineering (Vol. 8, No. 2, pp. 568-571). De Gruyter.

[11] Gyöngy, M., & Coussios, C. C. (2010). Passive cavitation mapping for localization and tracking of bubble dynamics. The Journal of the Acoustical Society of America, 128(4), EL175-EL180.

Neural networks meet magneto-mechanics: A framework for automated model generation

K.A. Kalina[1], P. Gebhardt[2], J. Brummund[1], W. Sun[3], M. Kästner[1]

[1] *Chair of Computational and Experimental Solid Mechanics, TU Dresden, 01062 Dresden, Germany.*
[2] *Chair of Mechanics of Multifunctional Structures, TU Dresden, Dresden, 01069, Germany.*
[3] *Department of Civil Engineering and Engineering Mechanics, Columbia University, New York, NY 10027, USA.*

Constitutive modeling is one of the pillars of continuum solid mechanics, which enables the mathematical description of different materials such as metals, rubbers or even active composites such as magnetorheological elastomers (MREs). In the history of constitutive modeling, considerable efforts were made to understand what physical conditions a constitutive model should fulfill, e.g., thermodynamic consistency and objectivity. While most conventional models proposed in the last decades were carefully formulated to fulfill these conditions, they have one major drawback: Based on a human choice of model equations, they are mostly limited to simple, only moderately flexible functional relationships. Due to that, alternatives based on machine learning are becoming increasingly popular, with neural networks (NNs) accounting for underlying physics being the most widely used.

Physics-augmented neural networks

In the first part, we introduce the concept of physics-augmented neural networks (PANNs), an approach which consequently accounts for physical conditions a priori, i.e., by construction [1]. This new family of NN-based constitutive models is discussed using isotropic hyperelasticity as an example. We train the model with ground truth data generated from a neo-Hooke model and consider interpolation as well as extrapolation behavior. An extension of the PANN model to anisotropic elasticity [2], viscoelasticity [3] or plasticity is also possible but nor discussed further here.

Application to magneto-mechanics

In the second part, we extend the PANN framework to finite strain magneto-elasticity [4]. Databases for training of the models are generated via computational homogenization for quasi-incompressible MREs. To reduce the computational cost, 2D statistical volume elements (SVEs) and a problem-specific sampling technique for the pre-selection of relevant states are used. The PANN model is then calibrated by using the database, whereby interpolation and extrapolation are considered separately. The numerical study suggests that the proposed PANN approach is advantageous over conventional models for MREs.

Acknowledgments

This work was supported by a postdoc fellowship of the German Academic Exchange Service (DAAD). This support is gratefully acknowledged. The authors also thank the German Research Foundation (DFG) for the support within the Research Training Group GRK 2868 D^3.

References

[1] L. Linden, D. K. Klein, K. A. Kalina, J. Brummund, O. Weeger, M. Kästner, Neural networks meet hyperelasticity: A guide to enforcing physics, *Journal of the Mechanics and Physics of Solids* 179 (2023) 105363.

[2] K. A. Kalina, L. Linden, J. Brummund, M. Kästner, FE^{ANN}: An efficient data-driven multiscale approach based on physics-constrained neural networks and automated data mining*, Computational Mechanics* 71 (2023) 827.

[3] M. Rosenkranz, K. A. Kalina, J. Brummund, W. Sun, M. Kästner, Viscoelasticty with physics-augmented neural networks: Model formulation and training methods without prescribed internal variables, *Computational Mechanics* (2024).

[4] K. A. Kalina, P. Gebhart, J. Brummund, L. Linden, W. Sun, M. Kästner, Neural network-based multiscale modeling of finite strain magnetoelasticity with relaxed convexity criteria, *Computer Methods in Applied Mechanics and Engineering* 421 (2024) 116739.

Superparamagnetic Nanoparticles in Magnetic Drug Targeting and Molecular Communication

J. Kirchner[1,2]

[1] *Lehrstuhl für Technische Elektronik (LTE), Friedrich-Alexander-Universität Erlangen-Nürnberg (FAU)*
[2] *Professur für Elektronik in der Medizintechnik, Fachbereich Informationstechnik, Fachhochschule Dortmund*

Superparamagnetic Iron-oxid Nanoparticles (SPIONs)

Superparamagnetic iron-oxid nanoparticles (SPIONs) consist of a magnetically active core of iron oxide and a coating to ensure colloidal stability and to functionalize the particle surface (see Fig. 1). Particle sizes for medical applications typically vary from 10 nm to 200 nm [1].

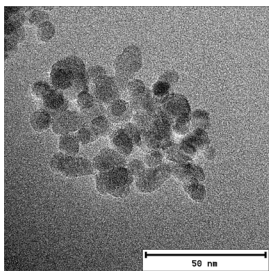

Figure 1: SPION sample, synthesized by the Section for Experimental Oncology and Nanomedicine (SEON) of the University Hospital Erlangen.

The property of superparamagnetism, i.e. a high susceptibility and no remanence, entails a strong interaction with magnetic fields but avoids particle accumulation in the absence of an external field. Together with their biocompatibility, this makes SPIONs suitable for a wide range of medical applications such as magnetic drug targeting and molecular communication.

SPIONs in Magnetic Drug Targeting

In magnetic drug targeting (MDT), SPIONs are used as carriers for tumor medication. By attracting the particles towards the tumor by use of a strong electromagnet, the fraction of the drug that reaches the target region is increased, thus improving therapeutic success and at the same time reducing adverse effects [2].

SPIONs in Molecular Communication

SPIONs can also be used to carry information, e.g., about insulin dosage between an implanted glucose sensor (transmitter) and an insulin pump (receiver). This is a particular example of molecular communication (MC), where information is transmitted by use of molecules and nano-size particles. MC provides an alternative to conventional data transmission based on electromagnetic fields, in situations where the latter is not applicable, e.g., due to strong signal attenuation, as is the case in the human body [3]. In fact, MDT can be interpreted as a form of MC, both aiming at maximizing the received signal in the target region. In this way, MDT and MC can benefit from each other, and particularly SPION-based testbeds provide means for studying processes and techniques for both contexts [4].

SPION Detection

SPION concentrations were initially measured inductively by use of susceptometers, conceived for characterizing material probes. In recent years, this measurement concept was advanced for application in MC and MDT research [5]: An increased temporal resolution allows to investigate time-varying SPION concentrations. Custom-made coils (Fig. 2) enable adaptation of the sensor to different channel geometries; in particular, planar coils facilitate the application in the human body [6]. Furthermore, by placing several sensors around the channel, information about the SPION distribution across the channel cross-section is obtained [7].

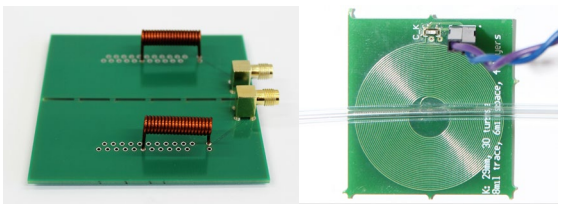

Figure 2: Inductive sensors with cylindrical and flat coil.

An alternative measurement approach is the use of capacitive sensors (see Fig. 4), which exhibit a larger signal-to-noise ratio than in the inductive approach but slower responses [8]. Furthermore, they promise a reduced sensitivity to electromagnetic interference, as needed in an MDT setup.

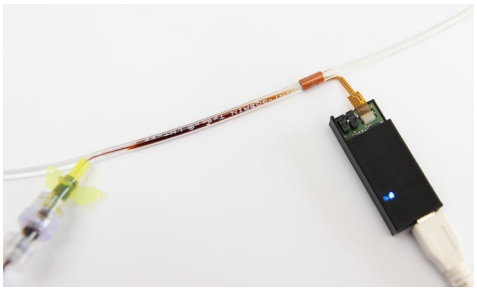

Figure 3: Injection of SPIONs into a silicone tube and sensing with an inductive and a capacitive sensor.

SPION Steering

The feasibility of particle steering at tube branchings has been demonstrated experimentally by several research groups [9,10]. The results from our measurements with a custom-made electromagnet at a branching are shown in Fig. 4 [7]. The difference of susceptibility, hence of SPION concentration, between the two channels behind the branching is shown in relation to the applied magnetic flux density, for different flow velocities.
For magnetic flux densities < 300 mT, the setup successfully directs more particles into the target branch, with the effect increasing with increasing magnetic field. A larger field strength, however, causes an accumulation of the particles in the vicinity of the electromagnet and thus diminishes the steering effect. Both effects are more pronounced the smaller the fluid flow is. Hence, an optimum has to be found between steering and avoidance of SPION accumulation.

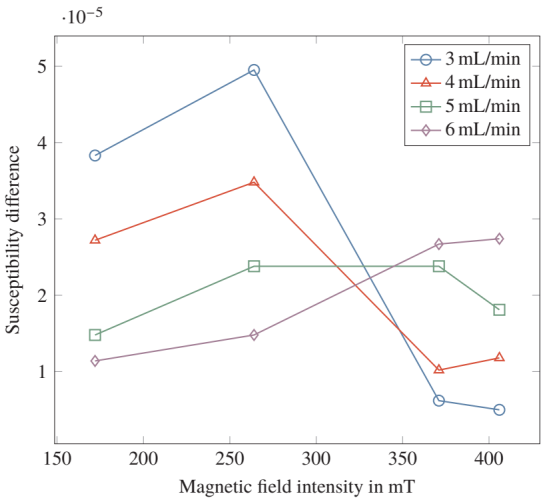

Figure 4: Results of the SPION steering setup.

What's Next?

In conclusion, both animal studies [2] and lab measurements [7,9,11] have demonstrated the feasibility and effectiveness of MDT and MC, two related approaches highly desired for medical use. For optimal results, the steering/communication setup has to be adapted to the complex individual geometry and flow profile of the transmission channel. However, both a systematic investigation of the physical and particularly biological processes, i.e., a comprehensive model, and effective algorithms for optimizing the parameters of the steering setup with respect to the SPION concentration in the target region are still missing. Such a model plus optimization algorithm has to capture the full complexity of the channel, with respect to both the vascular structure and the involved bio-physical processes, and at the same time, be computationally manageable. If these challenges can be solved, MDT and MC will improve cancer treatment and open up new applications of SPIONs in medical care.

References

[1] M. Mahmoudi et al., "Superparamagnetic iron oxide nanoparticles (SPIONs): development, surface modification and applications in chemotherapy", Adv. Drug Delivery Rev. 63(1-2), 24–46, 2011.

[2] R. Tietze et al., "Efficient drug-delivery using magnetic nanoparticles–biodistribution and therapeutic effects in tumour bearing rabbits", Nanomed. Nanotechnol. Biol. Med. 9(7), 961–971, 2013.

[3] T. Nakano, "Molecular communication", Cambridge: Cambridge University Press, 2013.

[4] S. Lotter et al., "Experimental Research in Synthetic Molecular Communications", IEEE Nanotechnol. Mag. 17(3), 42-65, 2023.

[5] M. Bartunik, G. Fischer, J. Kirchner, "The Development of a Biocompatible Testbed for Molecular Communication with Magnetic Nanoparticles", IEEE Trans. Mol. Biol. Multi-Scale Commun. 9(2), 179-190, 2023.

[6] M. Bartunik et al., "Planar coils for detection of magnetic nanoparticles in a testbed for molecular communication", Proc. 9th ACM Int. Conf. Nanoscale Comput. Commun. (NANOCOM '22), Barcelona, Spain, Oct. 5–7, 2022.

[7] M. Bartunik, "Practical Molecular Communication: The Development of two Testbeds," Dissertation, Friedrich-Alexander-Universität Erlangen-Nürnberg (FAU), 2023 (to be publ.).

[8] M. Bartunik, J. Reichstein, J. Kirchner, "Capacitive Sensing for Magnetic Nanoparticles in Molecular Communication", 2022 IEEE Int. Instr. Meas. Technol. Conf. (I2MTC), Ottawa, Canada, May 16–19, 2022.

[9] K. Gitter, S. Odenbach, "Experimental investigations on a branched tube model in magnetic drug targeting", J. Magn. Magn. Mater. 323(10), 1413–1416, 2011.

[10] A. K. Hoshiar et al., "Swarm of magnetic nanoparticles steering in multi-bifurcation vessels under fluid flow", J. Micro-Bio. Robot 16, 137–145, 2020.

Shape-dependent magnetic properties of hematite nanospindles

J. Kopp[1], G. Richwien[2], M. Heidelmann[3], S. Salamon[1], B. Rhein[2], A. M. Schmidt[2], J. Landers[1]

[1]*Faculty of Physics and Center for Nanointegration Duisburg-Essen (CENIDE), University of Duisburg-Essen*
[2]*Department for Chemistry and Biochemistry, University of Cologne*
[3]*ICAN, Interdisciplinary Center for Analytics on the Nanoscale*

Abstract

While it has been known for a long time that the aspect ratio of hematite nanospindles can be tuned by the synthesis parameter, the impacts on the magnetic properties are yet to be unraveled. The detailed investigation of the interplay between shape, aspect ratio, geometric and magnetic anisotropy provides important information on the influence of the geometry on the Morin transition.
For this reason, hematite nanospindles with different aspect ratios between 1.0 and 5.2 were prepared according to the method of Ozaki et al [1]. Transmission electron microscopy (TEM) analyses show that the particles grow along the c-axis, so that the short axis displays relatively small variations. This implies that the volume of the particles grows proportionally with increasing aspect ratio. The structural properties of the system were examined via HRTEM and XRD, revealing a well-defined crystal structure despite being composed of smaller primary subunit particles. To further study the magnetic properties, we performed Mössbauer spectroscopy and vibration sample magnetometry (VSM) measurements. In the zero-field-cooling/field-cooling (ZFC-FC) curves as well as in the Mössbauer spectroscopy results, we observe a gradual suppression of the Morin transition in hematite nanospindles for particles with high aspect ratio. This contradicts what has been reported earlier for the Morin transition that was observed to scale with the size of the particles [2-4].

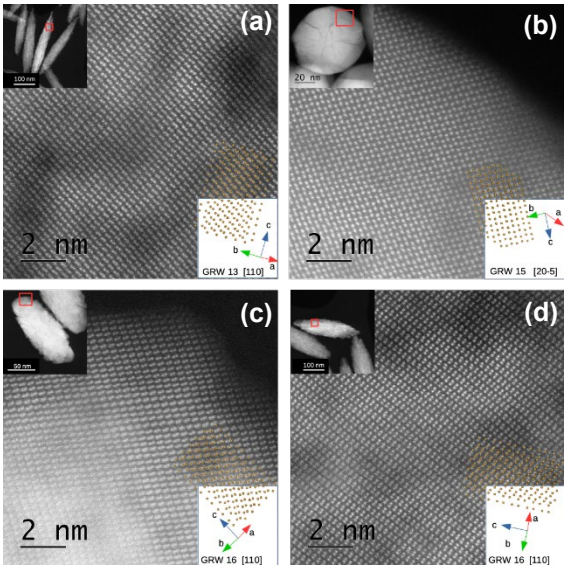

Figure 1: HRTEM analysis of the particles with the following aspect ratios: a) 5.2 b) 1.0 c) 2.5 d) 3.8

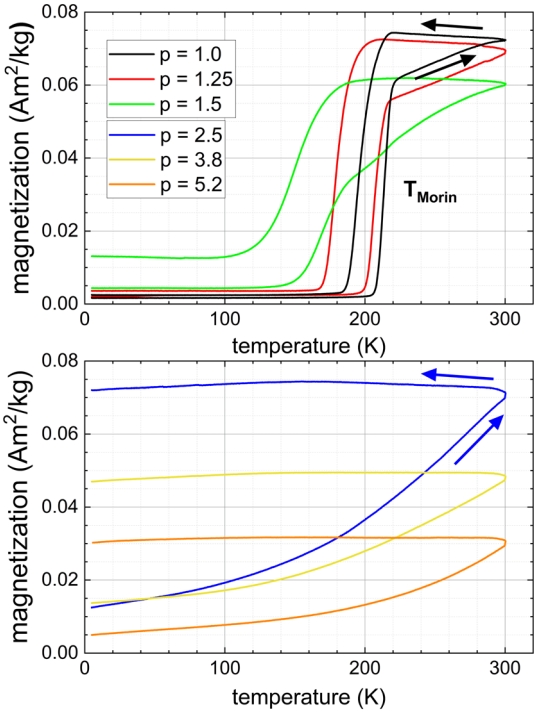

Figure 2: Zero-field-cooled/Field-cooled (ZFC-FC) curves for hematite nanospindles with different aspect ratios

We also see that for particles with an aspect ratio of 2.5 and above, the Morin transition is so strongly suppressed that it can no longer be observed even at temperatures down to 4 K, as shown in figure 2 and figure 3a.

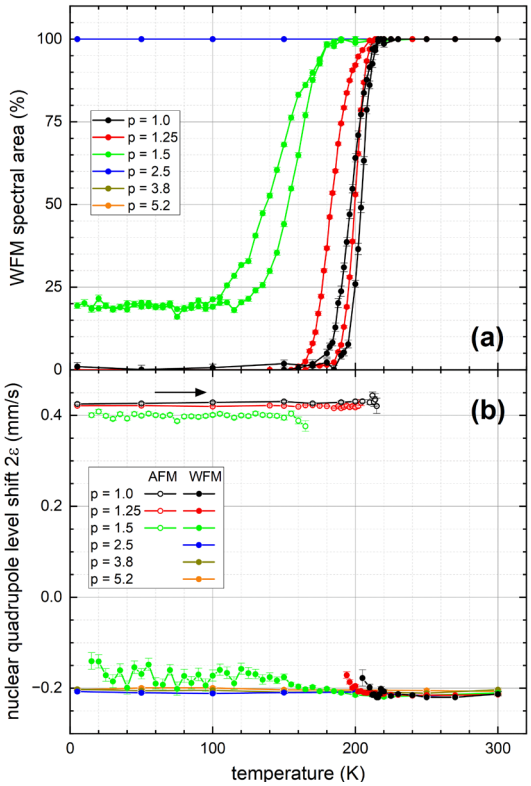

Figure 3: a) Spectral area of the weak ferromagnetic (WFM) contribution in the Mössbauer spectra together with b) the nuclear quadrupole level shift 2ε derived from the Mössbauer fit model

In addition, we observed a widening of thermal hysteresis and verified intermediary spin alignment states, deviating from the ideal 0° antiferromagnetic (AFM) or 90° weak ferromagnetic (WFM) spin structure for the sample p =1.5 (fig. 3b), connected to the Morin transition suppression for particles of a critical aspect ratio.

Outlook

This work demonstrates that the Morin transition can be tailored by altering the aspect ratio of hematite nanospindles. Furthermore, the results indicate that the physics of the Morin transition are not yet fully understood and more in-depth insights into its origin are needed. For this reason, in addition to the temperature-dependent results, the field-dependent data should provide an even more precise theoretical basis for the shape dependence of the Morin transition. The current field-dependent data already reveal interesting aspects that focus on the role of shape and magnetocrystalline anisotropy. The future task will be to refine the currently available theoretical models of this transition process.

Acknowledgments

Support by the Interdisciplinary Center for Analytics on the Nanoscale (ICAN) of the University of Duisburg-Essen (DFG RI sources reference: RI_00313), a DFG-funded core facility (Project Nos. 233512597 and 324659309), is gratefully acknowledged.

This work was financially supported by the DFG (projects LA5175/1-1 and SCHM1747/16-1)

References

[1] M. Ozaki, S. Kratohvil, and E. Matijevic, *Formation of Monodispersed Spindle-Type Hematite Particles,* **Journal of Colloid and Interface Science, 102(1)**, 146-151 (1984)

[2] D. Kubániová, L. Kubíčková, T. Kmječ, K. Závěta, D. Nižňanský, P. Brázda, M. Klementová, J. Kohout, *Hematite: Morin temperature of nanoparticles with different size,* **Journal of Magnetism and Magnetic Materials, 475**, 611-619 (2019)

[3] Ö. Özdemir, D.J. Dunlop, and T.S. Berquó, *Morin transition in hematite: Size dependence and thermal hysteresis,* **Geochemistry Geophysics Geosystems, 9,** Q10Z01 (2008)

[4] R. D. Zysler, D. Fiorani, A. M. Testa, L. Suber, E. Agostinelli, and M. Godinho, *Size dependence of the spin-flop transition in hematite nanoparticles,* **American Physical Society Physical Review B, 68,** 212408 (2003)

Particle interaction in heat transfer in ferrofluids

M. Krichler[1,2], S. Odenbach[2]

[1] *Bilfinger Nuclear & Energy Transition GmbH*
[2] *Chair of Magnetofluiddynamics, Measuring and Automation Technology, TU Dresden, 01062 Dresden, Germany*

Nanofluids are colloidal suspensions of particles in the order of nanometers to micrometers [1]. Ferrofluids can be regarded as a subcategory in which the particles (a) are magnetizable, (b) usually have a steric coating for long-term stabilization, and (c) cause paramagnetic properties in the suspension on a macroscopic level. In both, nanofluids in general and ferrofluids in particular, the potential for modifying thermal conductivity is under investigation. However, the underlying mechanisms are not yet fully understood, which leads to an insufficient ability to tailor suspensions to specific needs.

For nanofluids, research is dominated by application-oriented trial and error approaches with the aim of maximizing the increase in thermal conductivity [3]. The commonly used approach for approximating the thermal conductivity as a function of the quantity of suspended material, the Maxwell approximation [4], specifies two reference curves that enclose the expectation range for the increase in thermal conductivity. The Maxwell upper bound corresponds to the solid particles creating contiguous structures that divide the liquid phase into non-interacting areas. On the other hand, the Maxwell lower bound neglects any kind of particle interaction. In real fluids both bounds are just special cases. It can be assumed that, driven by chemical properties, electrostatic, magnetic, gravitational or temperature fields, processes of agglomeration, sedimentation and breaking-up into individual particles occur simultaneously [5].

Considering the missing steric surfactant, which leads to unpredictable interparticle interaction, it seems realistic that it is hardly possible to predict the thermal conductivity in nanofluids to a narrow degree just based on their composition.

For given reasons, the conditions for obtaining reproducible measurement results should be better in ferrofluids. In contrast to the nondirectional and hardly controllable impact of the suspended component on the thermal conductivity in nanofluids, the thermal conductivity in ferrofluids can be influenced by external magnetic fields.

However, experimental results are not unambiguous. [6], [7] and [8] could not measure any impact. [9] and [10] were able to detect an anisotropic change, while [11], [12] and [13] detected changes in parallel alignment of magnetic field and heat flow, only. It is unclear whether divergent effects were observed in the experimental investigations or whether the sensitivity of the measuring apparatus was just insufficient in those cases were no impact was noticed.

Nonetheless, due to the more precise synthesis and the ability for controllable magnetic interparticle interaction, ferrofluids are well suited to serve as a model system for the investigation on influencing factors on changing thermal conductivity.

In order to gather impact factors on changing thermal conductivity in ferrofluids, measurements were done with random ferrofluids, initially. Based on the heterogeneous findings a batch of ten tailored ferrofluids was investigated. Particle size distribution d, volume concentration φ, surfactant length δ, and viscosity η were altered both ways relative to a standard fluid. In all fluids thermal conductivity was increased parallel to an external, homogeneous magnetic field and lowered perpendicular to it. In each fluid the magnetic anisotropy was depending on the magnetic field strength. Relative to the results in the standard fluid, the effect was amplified in those fluids with bigger particles, higher concentration, shorter surfactant, and lower viscosity of the base fluid. The latter two could be considered surprising as both are not affected by magnetic fields. This draws the attention to the surfactant length and the base fluid

which are often ignored in investigations of interparticle interaction.

The diffusion coefficient of particles in a carrier liquid can be derived from Stokes' law on hydraulic resistance and written as

$$D_D = \frac{k_B \cdot T}{3 \cdot \pi \cdot \eta \cdot (d+2\delta)} \qquad (1)$$

One can extend the well-known [14] qualitative relation for interparticle interaction

$$\lambda^* = \frac{\mu_0 \cdot M_0^2 \cdot V}{24 \cdot k_B \cdot T} \cdot \left(\frac{d}{d+2\delta}\right)^3 \qquad (2)$$

and consider the volume fraction of suspended magnetic particles φ, too:

$$\lambda_{ID}^* = \varphi \cdot \lambda^* \cdot D_D \qquad (3a)$$

$$\lambda_{ID}^* = \varphi \cdot \frac{\mu_0 \cdot M_0^2}{432 \cdot \eta} \cdot \frac{d^6}{(d+2\delta)^4} \qquad (3b)$$

Doing so, all four investigated factors mentioned above are considered in this new parameter for interparticle interaction λ_{ID}^*. The measurement results appear to follow a pattern (Fig. 1), although a few results still do not match with it. However, this correlation is by far the best fit compared to λ^* or φ alone, or any other combinations of these, yet.

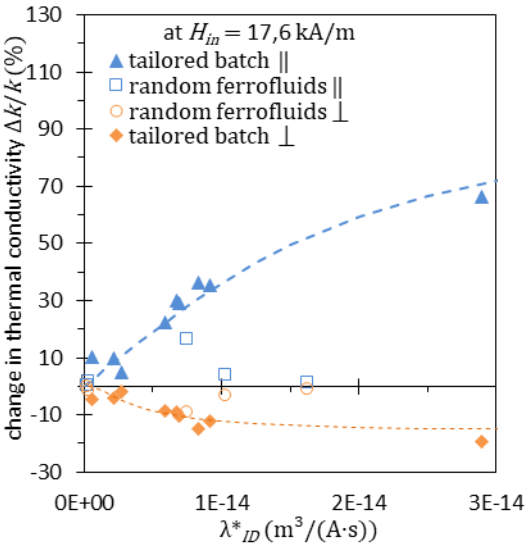

Figure 1: Measured values of change in thermal conductivity drawn over interparticle interaction parameter λ_{ID}^*. Both alignments, parallel and perpendicular to an external magnetic field are shown. The lines are just a guide for the eye.

The findings indicate that the carrier liquid and the surfactant, which both are not affected by magnetic fields, affect the magnitude of magnetic anisotropy and thus have to be taken into account in considerations on interparticle interaction.

One can fit the measured results of the tailored batch, for which the shown correlation matches well, and take magnetic field strength H_{in} into account:

$$\frac{\Delta k}{k} = \lambda_{ID}^* \cdot H_{in} \cdot g_{\lambda H} \qquad (4)$$

In this empiric approximation $g_{\lambda H}$ is a proportional factor received from first plotting $\Delta k/k$ over λ_{ID}^* and then plotting the found fit parameters over H_{in}. The derived value equals to $g_{\lambda H} = 2{,}209 \cdot 10^{12}\,\mathrm{s/m^2}$. This allows correlating the change in thermal conductivity of any fluid of the tailored batch for a given magnetic field strength.

A comparison of the results will be given to the approximation of Blums [15].

Acknowledgments

Financial support by *Deutsches Zentrum für Luft- und Raumfahrt* under grant number DLR 50 WM 0639 and DLR 50 WM 1235 is gratefully acknowledged.

References

[1] S. Choi, E. Eastman *ASME International mechanical engineering congress and exhibition*, San Francisco (1995)
[2] S. Odenbach, „Magnetoviscous effects in ferrofluids" (2002)
[3] E. Okonkwo, et al. *J Therm Anal Calorim* **145**, 2817-2872, (2021)
[4] J. Garnett, *Trans R Soc A* **203**, 385-420 (1904)
[5] J. Eapen, et al. *J Heat Transfer* **132**, 102402, (2010)
[6] E. Blums, et al. *Magnetohydrodynamics* **13**(1), 22-27 (1977)
[7] G. Kronkalns *Magnetohydrodynamics* **13**(3), 371-373 (1978)
[8] J. Popplewell, et al. *Colloid Polym Sci* **260**, 333-338 (1982)
[9] Z. Shul'man, et al. *J Eng Phys* **32**, 539-542 (1977)
[10] M. Krichler, S. Odenbach *J Magn Magn Mater* **360**, 85-90 (2013)
[11] Q. Li, et al. *Exp Therm Fluid Sci* **30**(2), 109-116 (2005)
[12] J. Philip, et al. *Appl Phys Lett* **92**, 043108 (2008)
[13] I. Nkurikiyimfura, et al. *International Conference on Materials for Renewable Energy & Environment*, Shanghai (2011)
[14] R. Rosensweig, "Ferrohydrodynamics" (1985)
[15] E. Blums, et al. "Magnetic Fluids" (1997)

Coarsening Dynamics of Ferromagnetic Granular Networks Under Variation of the Acceleration Amplitude

A. Lakkis[1], O. Bilous[2], P.A. Sanchez[2], S.S. Kantorovich[2] and R. Richter[1]

[1]*Experimentalphysik V, Universtät Bayreuth, 95440 Bayreuth (Germany)*
[2]*University of Vienna, Sensengasse 8, Vienna, 1090 Austria*

Introduction

Magnetised steel spheres self-assemble due to anisotropic magnetic interactions. If one shakes a mixture of glass and steel beads with a supercritical vibration amplitude, inter-particle collisions hinder the aggregation and keep the mixture in a "gas phase" [1]. Below a critical vibration amplitude, magnetic forces lead, first, to the formation of individual chains and rings that merge into a network [2] as the system relaxes as shown in Fig. 1. If given enough time, the network eventually compacts into crystalline-like islands of magnetic beads.

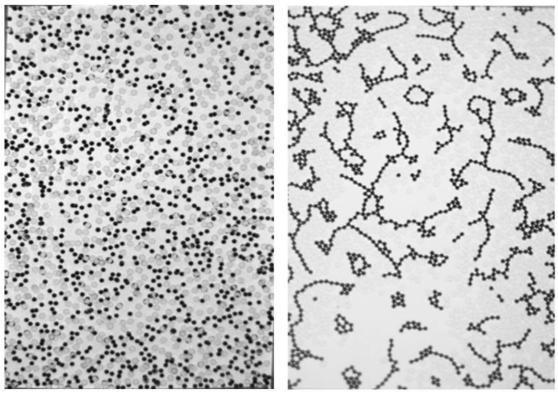

Figure 1 Snapshot of the coarsening dynamics after a quench of the vibration amplitude from 3g to 1.93g. Gas phase (a) and transient networks (b). From [2].

This scenario resembles the viscoelastic phase separation (VPS) introduced by Tanaka [3] for molecular mixtures. There phase separation arises from the different shear viscosities of both components, labelled as dynamic asymmetry by Tanaka. Also, in our mixture magnetic forces rise the shear viscosity of the ferrogranulate in contrast to the glass phase. And indeed, in experiments and computer simulations we found some evidence that the coarsening dynamics can be describes as a VPS in the macroscale [3]. A homogeneous magnetic field oriented in vertical direction was shown (in experiment and in silico) to hinder the coarsening dynamics [5,6]. This is, because the magnetized steel spheres eventually repel each other.
Likewise, the value of the under critical acceleration amplitude Γ plays a crucial role for the type of emerging pattern [1]. In the following we examine the coarsening dynamics for different values of Γ.

Experiment

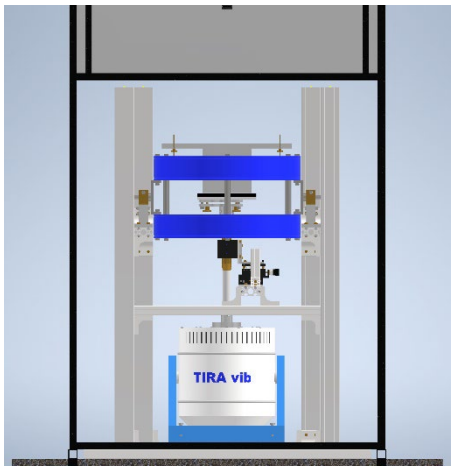

Figure 2. Scheme of the experimental setup.

A computer-controlled signal generator feeds a sinusoidal voltage signal into an amplifier which drives a vibration exciter from TIRA vib Co. The vibrations are coupled via a long rod (guided by a precision air

bearing) to the experimental vessel to avoid the magnetic stray field of the exciter. The vessel is filled with glass and steel beads. Pictures are recorded by means of a triggered camera. A Helmholtz-pair-of-coils (marked blue) serves to apply a vertical magnetic field. The setup is mounted on a stone plate (m=1.6t) which is floating on 4 air springs and can be levelled to 10 micrometer.

Experimental Results

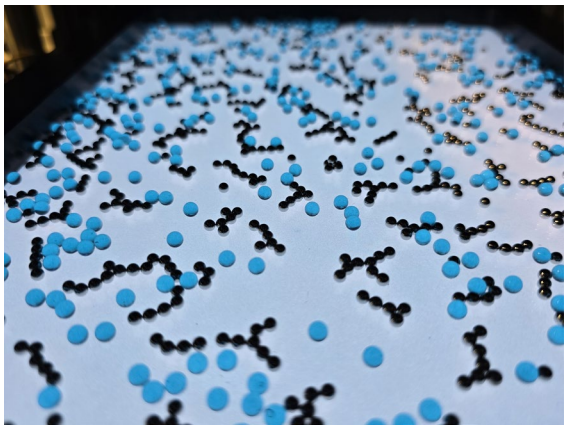

Figure 3. Snapshot of the dynamics.

Because the steel spheres are opaque (cf. Fig. 3) they can be easily tracked on the luminescent sheet. Figure 4 displays a characteristic velocity distribution, where the sharp peak in [0,1]mm/s stems from the beads in a cluster. Not yet agglomerated beads give rise to the broad distribution.
By utilizing blue glass beads (cf. Fig. 3) not only the steel but also the glass beads can be tracked.

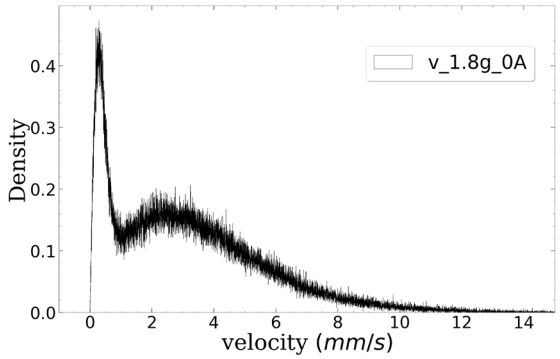

Figure 4. Velocity distribution of steel beads at 1.8 g recorded for 20 sec.

The mean degree of a node of the network, $\bar{k}$, has been proven to be a suitable order parameter [2,4,5]. We measure and analyze $\bar{k}$ (Γ) and compare the impact of a reduced Γ with the effect of an applied vertical induction.

Numerical Results

We study ferrogranulate via *molecular dynamics simulations* with a Langevin thermostat with a minimal coarse-grained model. In this model the spheres carry a magnetic point dipole in their centers. Our preliminary work [2,4] shows that to reproduce the susceptibility of the steel spheres it is sufficient as a first approach to introduce an additional central attraction (scaled by ε) between the steel spheres what we call here a *Stockmayer Granulate*. In simulations we treat the mechanical shaking as thermal fluctuations. The simulations are carried out with the package ESPResSO 4.1.4 [5].

Acknowledgments
The authors acknowledge financial support of the German-Austrian project “Coarsening dynamics of ferromagnetic granular networks – experiment and simulation” via Ri 1054/7-1 and I5160 FWF.

References

[1] D.L. Blair and A. Kudrolli, *Phys. Rev. E* 67 (2003) 021302.

[2] A. Kögel, P. Sanchez, R. Maretzki, T. Dumont, E. S. Pyanzina, S. S. Kantorovich, and R. Richter. *Soft Matter*, 14 (2018) 1001.

[3] H. Tanaka, *J. Phys: Condens. Matter* 12 (2000) R207.

[4] M. Biersack, A. Lakkis, R. Richter, O. Bilous, P.A. Sanchez, S.S. Kantorovich *Phys. Rev. E.* 108 (2023) 054905.

[5] A. Lakkis, M. Biersack, O. Bilous, S. Kantorovich, R. Richter, *J. Magn. Magn. Mater.* 589 (2024) 171620.

[6] – H. J. Limbach, A. Arnold, B. Mann, C. Holm, *Comput. Phys. Commun* 174 (2006) 704.

Tunable magnetic behavior in Pt@[$CoFe_2O_4$]$_n$ hybrid nanoparticles

J. Landers[1], M. A. Raphael[2], S. Salamon[1], H. Wende[1], A. M. Schmidt[2]

[1] *Faculty of Physics and Center for Nanointegration Duisburg-Essen (CENIDE), University of Duisburg-Essen*
[2] *Institute of Physical Chemistry, Chemistry Department, University of Cologne*

Introduction

Pt@[$CoFe_2O_4$]$_n$ (P*n*) hybrid nanoparticles represent a system with fascinating magnetic properties, governed by a sensitive interplay of magnetocrystalline (MCA), surface- and shape anisotropy, as well as intra- and interparticular magnetic interactions, which can be tuned via number, size and configuration of the utilized subunits: Depending on synthesis conditions, the hybrid nanoparticles consist of *n* 15 nm cobalt ferrite (CFO) nanocubes attached to a smaller central cubic Pt particle (Fig. 1). For details on synthesis parameters and particle morphology we refer to the contribution by M. A. Raphael, University of Cologne.

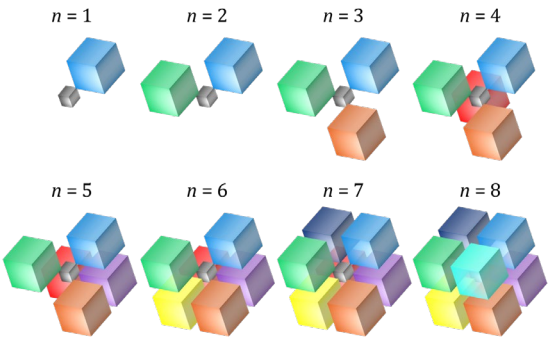

Fig. 1: Schematical particle geometry showing characteristic configurations of n CFO nanocubes (colored) around the central Pt subunit (grey).

Results and Discussion

For a general characterization of the particles' magnetic structure, hybrid particles with n = 1 (P1) and n = 3 (P3) were analyzed via in-field Mössbauer spectroscopy (see Fig. 2), revealing a ferrimagnetic state with low spin canting and an inversion parameter x ≈ 0.77. Based on this analysis, we would assign the nanoparticles a stoichiometry of $[Co^{2+}_{0.23}Fe^{3+}_{0.77}]_A(Co^{2+}_{0.77}Fe^{3+}_{1.23})_BO_4$, from which we can infer a saturation magnetization M_S of ca. 490 kA/m. As expected for cobalt ferrite, the particles show high coercive fields in magnetometry experiments, indicating a high effective magnetic anisotropy, especially at lower temperatures. This is accompanied by a mainly magnetically blocked state up to well above 300 K. Due to the small distance between CFO cubes, a strong intraparticular interaction leads to an increase in blocking temperatures when going from P1 to P3, accompanied by interparticle interaction depending on the average distance between the hybrid nanoparticles.[1]

Measurements of the thermoremanent magnetization as well as the temperature dependence of the squareness ratio M_R/M_S shown in Fig. 3 indicate distinct temperature regions with different characteristic magnetic behavior: While at low temperatures, M_R/M_S is close to values of 0.8, it decreases to about 0.5 at ambient temperature, in accordance with the standard Stoner-Wohlfarth model of uniaxial anisotropy. Only at even higher temperatures around 400 K does the magnetic behavior approach $H_C \approx 0$ towards the superparamagnetic regime.

We assign these observations to the predominantly cubic magnetocrystalline anisotropy reported for CFO with $K_1 > 0$ at low temperatures, resulting in the occurrence of magnetically easy axes along the

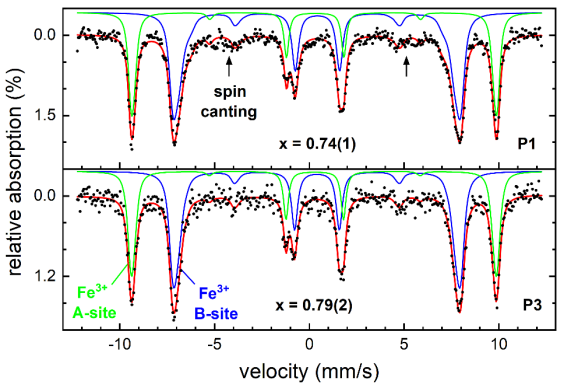

Fig. 2: Mössbauer spectra of Pt@[$CoFe_2O_4$]$_n$ hybrid particles P1 (top) and P3 (bottom), recorded at 5 K and 8 T, showing sextet subspectra of A-site (green) and B-site (blue) Fe^{3+}.

(100) axes of the nanocubes, with an expected $M_R/M_S \approx 0.831$.[2] The value of $M_R/M_S \approx 0.5$ at intermediate temperatures is interpreted to originate from an effective uniaxial anisotropy, [2,3] stemming, e.g., from interaction effects and contributions of shape anisotropy for slightly elongated cubes, the latter being less affected by elevated temperatures, presumably then becoming the predominant contribution to effective magnetic anisotropy.

This transition from cubic to uniaxial anisotropy is about 60 K lower for P3 in comparison to P1. This could potentially be explained by a preferred (111)-magnetic alignment induced by the hybrid particle shape anisotropy partially compensating MCA, leading to an earlier transition to hysteresis behavior governed by an effective uniaxial magnetic anisotropy.

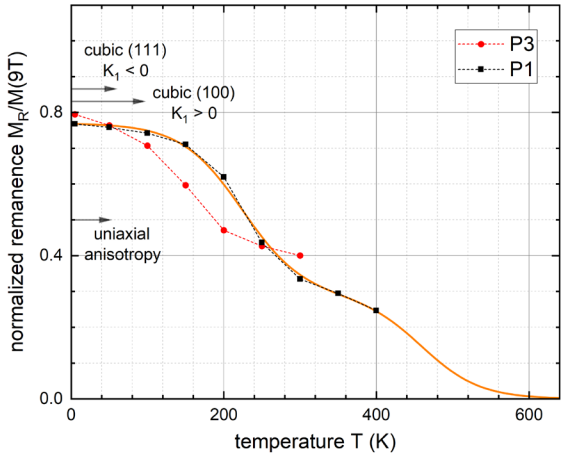

Fig. 3: Squareness ratio M_R/M_S approximated via $M_R/M_{(9T)}$ for P1 and P3. Arrows mark theoretical positions of M_R/M_S for different types of MCA, the orange line is a guide to the eye.

Conclusion

Pt@$[CoFe_2O_4]_n$ hybrid particles represent a magnetically blocked, high-anisotropy system, with properties that are widely tunable by the number and size of attached CFO nanocubes, potentially allowing distinct variations in the composition of different contributions to effective magnetic anisotropy, which could lead to new types of magnetic hysteresis behavior.

Acknowledgements

Financial support by the German Research Foundation (DFG) within projects SCHM1747/16-1 and LA5175/1-1 is gratefully acknowledged.

References

[1] J. Landers et al., *J. Phys.: Condens. Matter* **27**, 026002 (2015)

[2] M. P. Adams et al., *IUCrJ* **10**, 261-269 (2023)

[3] D. Faílde et al. *Nanoscale*, Advance Article (2024)

Graphical Magnetogranulometry applied to temperature-dependent magnetization curves

A. Lange[1], I. Rehberg[2]

[1] *TU Dresden, Institute of Mechatronic Engineering, Chair of Magnetofluiddynamics, Measuring and Automation Technology, D-01062 Dresden, Germany*
[2] *Institute of Physics, University of Bayreuth, D-95440 Bayreuth, Germany*

The magnetisation curve of the commercially available magnetic fluid APG513a is measured at five different temperatures. The curves can be described by the method of graphical magnetogranulometry [1, 2], which is accompanied by a fit to a superposition of four Langevin terms. The method yields the arithmetic and the harmonic mean of the particle distribution. It has an advantage compared to the fitting of magnetization curves to some appropriate mathematical model: It does not rely on assuming a particular distribution function of the particles.
Starting point is the measured magnetisation M_{mea} as function of externally applied magnetic field H_0. The Weiss correction $H_e=H_i+M/3$ is applied, where H_i denotes the magnetic field inside the sample. By exploiting the almost spherical geometry of sample holder, the fitting procedure yields the corresponding magnetisation M_{fit} versus $B_e/\mu_0=H_e=H_0$, see figure 4 in [1] and figure 1 in [2], respectively. The quality of the fitting procedure for a selected temperature of T=288 K in the initial region of H_e is shown in figure 1 and in the region beyond the initial range up to 800 kAm^{-1} in figure 2.

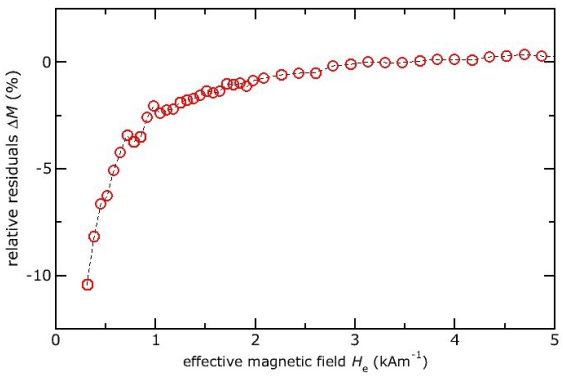

Figure 1: The relative residuals $\Delta M=(M_{fit}-M_{mea})/M_{mea}$ versus H_e for the initial region of H_e with $0 \le H_e \le 5$ kA m^{-1} at T=288 K. The dashed black line is just a guide to the eye.

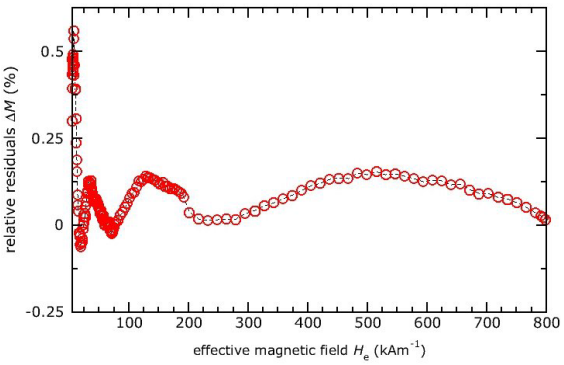

Figure 2: The relative residuals $\Delta M=(M_{fit}-M_{mea})/M_{mea}$ versus H_e with $5 \le H_e \le 800$ kA m^{-1} at T=288 K. The dashed black line is just a guide to the eye.

With a transformation back to H_i one gets the fitted magnetization M_{fit} versus H_i allowing a comparison with the initially measured magnetisation curve. Figure 3 shows the excellent agreement for the selected temperature T=288 K.

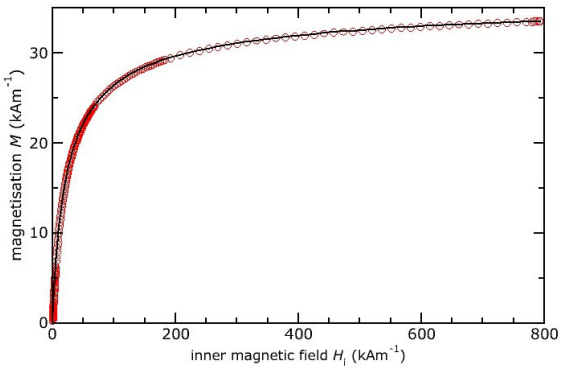

Figure 3: Magnetisation M versus H_i at T=288 K. The black solid line shows the fitted values $M_{fit}(H_i)$, the red circles the measured values $M_{mea}(H_i)$.

The quality of the agreement holds for all tested temperatures T=288 K, 293 K, 298 K, 303 K, and 308 K.

Based on the $M_{fit}(H_i, T)$ as well as on the $M_{mea}(H_i, T)$ curves, the contribution aims at a determination of the pyromagnetic coefficient of the magnetic fluid APG513a.

Acknowledgments

The authors acknowledge their thanks to Roland Mußbach who carried out the measurements of the magnetization.

References

[1] I. Rehberg, R. Richter, S. Hartung, N. Lucht, B. Hankiewicz, and T. Friedrich, Phys. Rev. B 100, 134425 (2019).

[2] I. Rehberg, R. Richter, and S. Hartung, J. Magn. Magn. Mat. 508, 166868 (2020).

Rheology of Blood-Diluted Ferrofluids

Z. Liu, D. Borin, S. Odenbach

Chair of Magnetofluiddynamics, Measuring and Automation Technology, TU Dresden, 01069 Dresden, Germany

Introduction

Magnetic Drug Targeting (MDT) is a novel technique for cancer treatment that uses ferrofluids containing magnetic nanoparticles (MNPs) and its surfactant to transport antibodies to specific tumor regions under a magnetically control. This technique greatly improves drug utilization efficiency and reduces the toxic side effects. Ensuring its safety is crucial, particularly regarding the changes in properties when ferrofluids mix with blood under magnetic field strength.
Several previous studies have explored the Magnetoviscous Effect (MVE) - the viscosity increase due to chain structures formed by MNPs - of ferrofluids diluted with blood to simulate the flow process after injecting ferrofluids with antibodies into blood vessels. However, these studies have yielded contradictory results regarding this effect. In this work, we conducted experiments to investigate whether an interaction between MNPs and blood components under a magnetic field is possible and observed the viscosity change over time.

Experiments

The experiments were carried out using a shear-rate controlled rheometer with a cone-plate setting, ensuring equal shear rates throughout the entire measuring zone. The biocompatible ferrofluid FluidMAG-D200 from Chemicell was used, with water as the carrier fluid and MNPs coated with starch. Sheep blood was chosen as the diluent due to its viscosity similarity to human blood and for better comparability with previous results.
The ferrofluids were diluted with sheep blood in different ratios. After magnetic characterization using a vibrating sample magnetometer (VSM), the samples were subjected to an external magnetic field generated by two parallel Helmholtz coils. Each test series started with lower shear rates, which were then incrementally increased. The shear stress was measured by a torque sensor and displayed. The MVE was calculated using the following equation [2]:

$$R = \frac{\eta_H - \eta_{H=0}}{\eta_{H=0}} \qquad (1)$$

For the time-dependent measurements, the samples were subjected to a constant magnetic field strength and shear rate for a period within a tolerable temperature range. The viscosity change of the mixture was then observed. Water was used as an additional diluent for comparison purposes.

Results

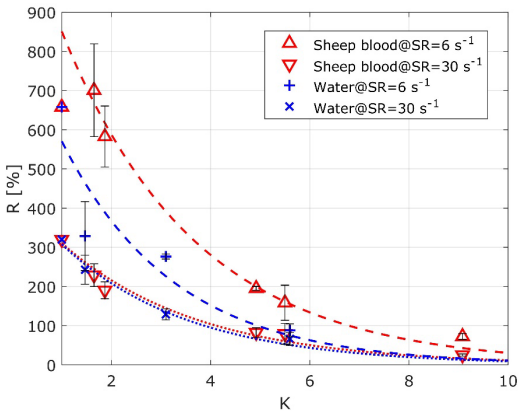

Figure 1. MVE as a function of the dilution factor K, comparison between sheep blood and water as diluent and shear rate $\dot{\gamma}$ of 6 and 30 respectively. All experiments were performed under a magnetic field strength of H=35kA/m.

Figure.1 shows the comparison of MVE between sheep blood and water. All data points were fitted using the following formula [3]:

$$R = R_0 \cdot \exp\left(-\frac{K-1}{p}\right) \qquad (2)$$

The results indicate that when the dilution factor is between 1 and 5, the MVE of

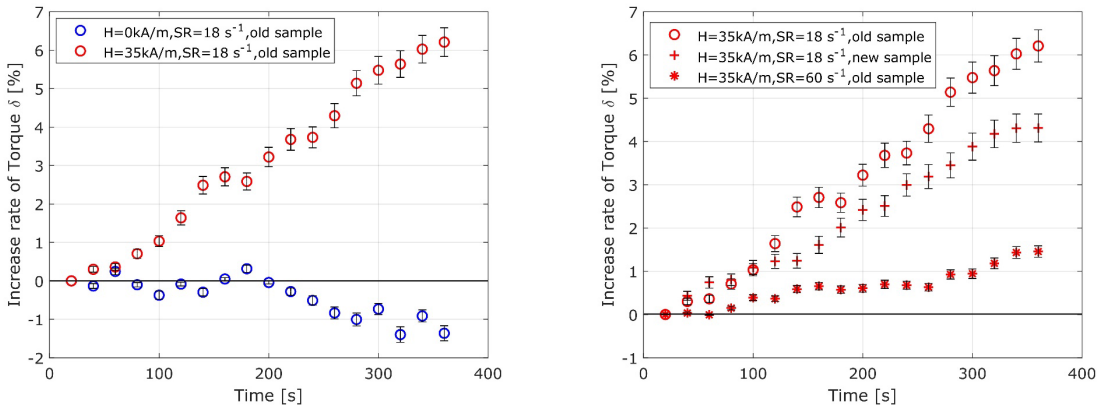

Figure 2. Increase rate of the torque δ over time with an external magnetic field, (a) the same sample with and without magnetic field strength and (b) comparison between different samples and shear rates with constant magnetic field strength of H =35kA/m.

sheep blood is significantly higher than that of water. This difference decreases with higher shear rate, which is reasonable because higher shear rates lead to stronger shear stress, causing the chain-like structures formed by MNPs to break down faster.

Figure 2. shows the increase rate of torque over time. From Figure 2(a), it is evident that the viscosity of the mixture continues to grow compared to the irregular behavior without magnetic strength, with no signs of stopping at the end of the period. Figure 2(b) demonstrates the repeatability of this phenomenon with both old and new samples under different shear rates.

Discussion

The observed MVE difference between ferrofluids diluted with sheep blood and water is undeniable. Combined with the experimental results showing the increase in torque over time, we boldly hypothesize that there may be an interaction between the MNPs and the red blood cells (RBCs), considering the iron content in whole blood.

There are two possible explanations: given that the volume of RBCs is much larger, they may absorb some tiny MNPs during the measurement period, resulting in the formation of extra chain structures that lead to continuously growing viscosity; alternatively, larger MNPs tend to aggregate after the magnetic influence, while smaller MNPs may adhere to the surface of the RBCs, and together they form chain structures when the magnetic field is reapplied.

Outlook

The results of this work indicate a high probability of interaction between RBCs and MNPs. Further experiments are necessary for a more reliable conclusion, including comparisons between blood and plasma and detailed microscopic observations.

References

[1] Gavas, S., Quazi, S., & Karpiński, T. M. (2021). Nanoparticles for cancer therapy: current progress and challenges. *Nanoscale research letters*, *16*(1), 173.

[2] Odenbach, S., & Thurm, S. (2002). Magnetoviscous effects in ferrofluids. In Ferrofluids: magnetically controllable fluids and their applications (pp. 185-201). Berlin, Heidelberg: Springer Berlin Heidelberg.

[3] Nowak, J., Nowak, C., & Odenbach, S. (2015). Consequences of sheep blood used as diluting agent for the magnetoviscous effect in biocompatible ferrofluids. Applied Rheology, 25(5), 1-8.

Dynamic magnetooptical response of a ferromagnetic liquid crystal

H. Nádasi[1], T. Smulovics[1,2], A. Eremin[1], D. Lisjak[3], M. Küster[4], F. Ludwig[4]

[1] *Institute of Physics, Otto von Guericke University Magdeburg, 39108 Magdeburg, Germany*
[2] *L. Miller–Great Neck North High School, New York, USA*
[3] *Jožef Stefan Institute Ljubljana, Ljubljana, Slovenia*
[4] *Institut für Elektrische Messtechnik und Grundlagen der Elektrotechnik und LENA, TU Braunschweig, Braunschweig, Germany*

A combination of the form-anisotropy of magnetic nanoplatelets (MNP) with magnetic and electrostatic interactions gives rise to a fascinating new system – liquid magnets [1,2]. Those systems, demonstrated by Mertelj et al., consist of the barium hexaferrite nanoplatelets (BaHF) nanoplatelets (NP) suspended in a nematic host and combine fluidity with the ferromagnetic order. In such ferromagnetic nematics (Nm), strong interparticle correlations induced by the particle-matrix coupling profoundly affect the dynamics of the MNPs, which are still not fully characterised. We explore the dynamic behaviour of the Nm in an external magnetic field in bulk and droplet geometry. External magnetic field couples to the nematic director, allowing control of the optical birefringence.

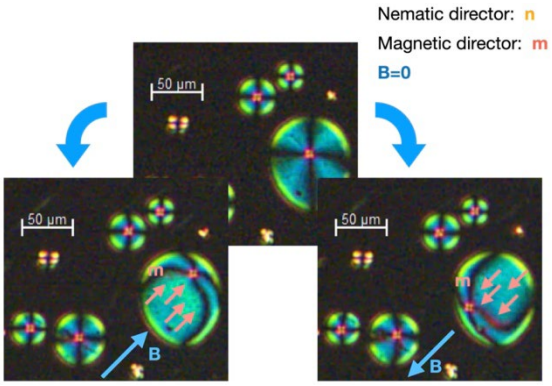

Figure 1. The effect of an external magnetic field on the topological defects in sessile Nm droplets.

In our experiment, we analyse the dynamics of the magnetooptical response in both the time and frequency domains by measuring the optical transmission of thin micrometre-sized samples between crossed polarisers. The response shows strong concentration dependence and is also influenced by the orientation of the applied magnetic field to the preferred alignment of the nematic director. When a magnetic field is rotated, soliton-like director structures emerge, displaying complex dynamic behaviour.

In liquid crystal droplets, the nematic director adopts the configuration determined by the boundary anchoring. The anchoring conditions can be controlled by selecting a suitable surfactant. In our study, we produced the sessile droplets with the radial director orientation in a homeotropic cell with CTAB treated substrates. The coupling between the magnetic and nematic directors allowed us to manipulate the topological defect using an external magnetic field (Figure 1). The defect motion confirmed the assumption of the ferromagnetic order with co-linear aligned nematic and magnetic directors. Additionally, we demonstrated that both parallel and antiparallel director configurations are possible.

Acknowledgments
This research was supported by the German Research Foundation DFG, (NA 1668/1-3, LU 800/7-1, and ER 467/8-3).

References

[1] A. Mertelj, et al., Nature **504**, 237 (2013).
[2] M. Shuai, et al., Nat. Comm. **7**, 10394 (2016).

Nonlinear optical and magneto-electric effect in multiferroic LC hybrids

H. Nádasi[1], A. Jarosik[1], A. Eremin[1], P. M. Rupnik[2], A. Mertelj[2], N. Sebastián[2], D. Lisjak[2], M. Küster[3], F. Ludwig[3]

[1] *Institute of Physics, Otto von Guericke University Magdeburg, Magdeburg, Germany*
[2] *Jožef Stefan Institute Ljubljana, Ljubljana, Slovenia*
[3] *Institut für Elektrische Messtechnik und Grundlagen der Elektrotechnik und LENA, TU Braunschweig, Braunschweig, Germany*

Suspensions of barium hexaferrite (BaHF) nanoplatelets (NP) in anisotropic hosts, such as nematic liquid crystals (LCs), are known to form liquids with ferromagnetic order [1,2]. The nematic order is crucial for the colloidal stabilisation of the suspension. Multiferroic materials exhibiting more than one ferroic type of order can be designed as hybrids containing BaHF NPs dispersed in a ferroelectric host. However, most of ferroelectric LCs are smectics, which do not form stable suspensions of nanoparticles.

The recent discovery of true ferroelectric 3D fluids, the ferroelectric nematics (N_F), has opened up new avenues for designing multiresponsive hybrid materials [5,6]. Our previous research demonstrated that multiferroic properties can be observed in room-temperature ferroelectric nematic phase doped with BaHF NPs. Here, we discuss the magneto-electric effect resulting from the coupling between the magnetic and ferroelectric types of order, where the external magnetic field can control the electric polarisation.

Using magnetic pulses, we measure the induced electric polarisation using transient currents induced in the sample. The current response is influenced by the NP concentration and sample preparation. One of the consequences of the vectorial order in the ferroelectric phase is the strong optical nonlinearity. The N_F materials exhibit high-efficiency optical second harmonic generation (SHG) comparable to that of solid ferroelectrics. The magneto-electric coupling enables the manipulation and tuning of SHG using external magnetic fields. These discoveries make fluid multiferroics promising for applications in nonlinear optics.

Acknowledgments
This research was supported by the German Research Foundation DFG, (NA 1668/1-3, LU 800/7-1, and ER 467/8-3) and the Slovenian Research Agency ARRS (P1-0192, J1-2459). The authors thank to Merck Electronics KGaA for the LC material.

References

[1] A. Mertelj, et al., Nature **504**, 237 (2013).
[2] M. Shuai, et al., Nat. Comm. **7**, 10394 (2016).
[3] X. Li, et al., Sci. Reports **13**(1), 1755 (2023)
[4] N. A. Spaldin, et al., Nat. Mat. **18**(3), 203 (2019)
[5] H. Nishikawa, et al., Adv. Mat. **29**(43), 1702354 (2017)
[6] Nádasi, et al., Nat. Mat., submitted (2024)

Impact of Coating Type on Structure and Magnetic Properties of Biocompatible Iron Oxide Nanoparticles: Insights into Cluster Organization and Oxidation Behaviour

A. Nasser[1,2], A. Qdemat[3], H. Unterweger[4], R. Tietze[4], X. Sun[5], J. Landers[6], J. Kopp[6], B. Wu[2], M.-S. Appavou[2], A. Murmiliuk[2], E.P. Gilbert[7], O. Petracic[3], A. Feoktystov[2]

[1] *Department of Physics, Technical University Munich (TUM), Garching, Germany*
[2] *Forschungszentrum Jülich GmbH, Jülich Centre for Neutron Science JCNS at MLZ, Garching, Germany*
[3] *Forschungszentrum Jülich GmbH, Jülich Centre for Neutron Science JCNS-2, Jülich, Germany*
[4] *ENT Department, Section of Experimental Oncology and Nanomedicine (SEON), Else Kroener-Fresenius-Stiftung-Professorship, University Hospital Erlangen, Germany*
[5] *Deutsches Elektronen-Synchrotron DESY, Hamburg, Germany*
[6] *Faculty of Physics and Center for Nanointegration Duisburg-Essen (CENIDE), University of Duisburg-Essen, Duisburg, Germany*
[7] *Australian Centre for Neutron Scattering, Australian Nuclear Science and Technology Organisation, Lucas Heights, Australia*

Superparamagnetic iron oxide nanoparticles (SPIONs) are promising nano-vehicles for biomedical applications such as drug delivery, imaging, and magnetic hyperthermia. However, one of the limitations of these systems is their tendency to agglomerate, which has a direct impact on the efficiency of their performance. One way to overcome this limitation is to apply a coating during synthesis. In this work, we have investigated the effect of three biocompatible coatings on controlling the agglomeration of iron oxide nanoparticles. The biocompatible coatings used are sodium citrate, (3-aminopropyl)triethoxysilane (APTES), and dextran. The structural and magnetic properties of the coated nanoparticles are characterized using various experimental techniques, including cryogenic transmission electron microscopy (cryo-TEM), magnetometry, Mössbauer spectroscopy, and small-angle X-ray and neutron scattering. The results show that the coatings effectively stabilize the nanoparticles, and lead to clusters of different sizes which then modifies their magnetic behaviour due to magnetic inter-particle interactions. We also investigated the oxidation kinetics of the nanoparticles prepared with the various coating materials as a function of time to characterize the oxidation behaviour and stability. This research provides valuable insights into the design of an optimized nanoparticle functionalization strategy for biomedical applications.

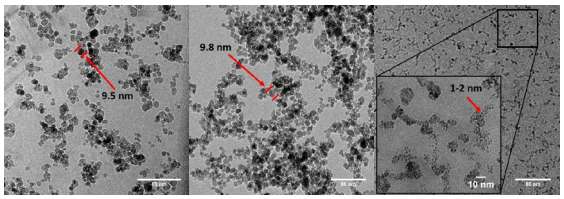

Figure. Cryo-TEM images of SPIONs with (a) sodium citrate, (b) APTES and (c) dextrane coating. Red arrows indicate single nanoparticles in the clusters. The size of the single nanoparticles is given exemplarily.

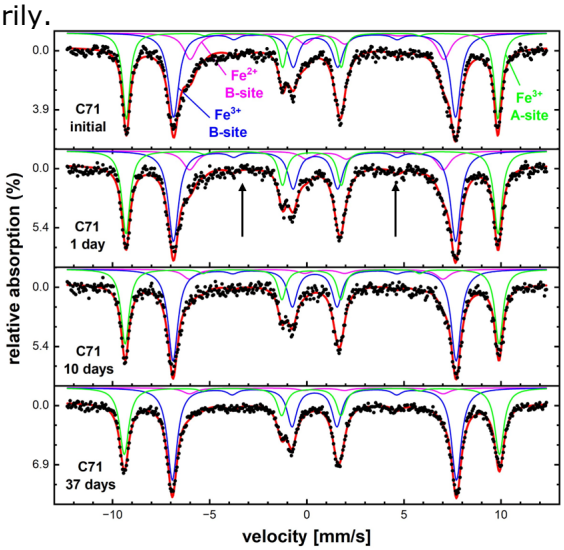

As an example, Mössbauer spectra for citrate sample after various aging times of exposure to air, recorded at 5 K and an applied magnetic field of 8 T. In the day 1 spectrum, the vertical arrows mark Mössbauer lines 2 and 5, whose relative intensity indicates the degree of spin canting.

Investigate the Polyaniline decorated Iron based Magnetorheological fluids with enhanced Viscoleastic properties

Noorjahan[1]

[1]Department of Physics and Astronomical sciences in Central University of Himachal Pradesh, India

Abstract

Enhancing the stability of Magnetorheological fluids (MRFs) has emerged as a major concern inhibiting their use in wide range of applications across various engineering fields. Introducing conductive polymers such as Polyaniline in these MRFs can serve the purpose of enhancing the sedimentation stability of these Magnetorheological fluids and also can benefit us with its conductive properties opening a pioneering stride in the field of smart materials. In light of this, we have prepared a novel class of MR fluids that incorporate polyaniline as a stabilizer into iron powder-based MR formulations, enhancing their long-term stability. This study deals with the synthesis, characterization, and rheological performance of polyaniline-modified iron powder-based MR fluids. For the synthesis of Polyaniline, chemical oxidative polymerization technique has been employed. X-ray diffraction confirmed the formation of Polyaniline and good crystalline nature of Iron. Microstructural and grain size information of Iron and Polyaniline has been obtained using the Field Emission Scanning Electron Microscope (FESEM). Matrix of irregular cauliflower shaped Polyaniline supports the iron particles ensuring the consistent Viscoleastic properties over extended period of time. This study also investigates the influence of magnetic field strength on the fluid's rheological response, offering insights to optimize performance for practical applications.

Rheological studies

Mason number, a dimensionless number defined as the ratio of hydrodynamic force and magnetic force plays an important role in the behavior of the MR fluids. It depicts the effect of the magnetic field on the chain structure.

$$M_n = \frac{\eta_c \dot{\gamma}}{2\mu_o \mu_c \beta^2 H^2}$$

Where, η_c is the continuous phase viscosity, which is silicone oil, μ_o is the permeability of vacuum, μc is the relative permeability of the continuous phase, β is a constant factor given by $\beta = \frac{\mu_p - \mu_c}{\mu_p + \mu_c}$ and carries a value between 2 to 3 for MRFs.

Figure 1 illustrates the variation of dimensionless relative viscosity, represented as η/η_∞, plotted against the Mason number (Mn) showing a decrease in relative viscosity with increasing Mason number. Notably, the absence of converged curves for relative viscosity versus Mason number at different magnetic fields is evident in the case of Fe fluid, as observed from Figure 1. In contrast, for FeP (2%) and FeP (4%) samples, the curve almost collapses into a single curve, indicating a balance between magnetic and hydrodynamic forces, with both forces exerting dominant influences.

Figures.1 Variation of relative velocity with mason number of Fe, FeP (2%) and (4%) MRFs

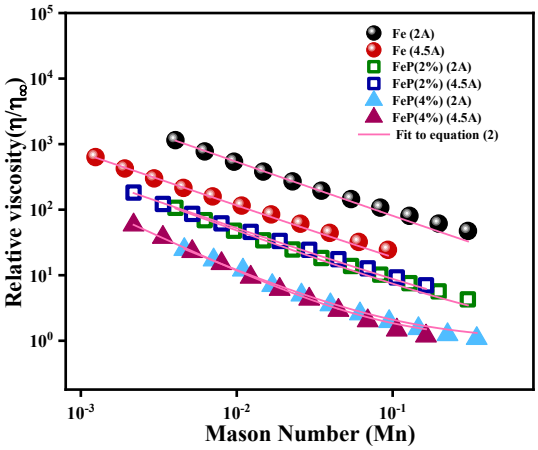

Acknowledgments

Noorjahan acknowledges the financial support provided by the Central University of Himachal Pradesh & UGC, India.

References

1. Noorjahan, S. Pathak, K. Jain, and R. P. Pant, "Improved magneto-viscoelasticity ofcross-linked PVA hydrogels using magnetic nanoparticles," *Colloids Surf. Physicochem.Eng. Asp.*, vol. 539, pp. 273–279, Feb. 2018, doi:0.1016/j.colsurfa.2017.12.011.
2. [2] R. Singh, S. Pathak, K. Jain, Noorjahan, and S.-K. Kim, "Correlating the Dipolar Interactions Induced Magneto-Viscoelasticity and Thermal Conductivity Enhancements in Nanomagnetic Fluids," *Small*, vol. 19, no. 39, p. 2205741, 2023, doi:10.1002/smll.202205741

Synthesis and characterization of multifunctional Pt@[$CoFe_2O_4$]$_n$ hybrid nanoparticles

M. A. Raphael[1], Y. Martinez[1], M. Effertz[1], J. Landers[2], S. Salamon[2], H. Wende[2], A. M. Schmidt[1]

[1] *Institute of Physical Chemistry, Chemistry Department, University of Cologne*
[2] *Faculty of Physics and Center for Nanointegration Duisburg-Essen (CENIDE), University of Duisburg-Essen*

Introduction

The combination of different components to hybrid-, heterofunctional nanostructures enables a synergy of material properties and thus multifunctionality. In the case of the Pt@[$CoFe_2O_4$]$_n$ (P*n*) nanoobjects, *n* cobalt ferrite (CFO) cubes are connected to a platinum cube via corner-to-corner junctions. These unique morphologies enable the combination of magnetic and plasmonic or catalytic functionality and they can be seen as model systems for the investigation of nanomagnetic interactions.

Results and Discussion

The synthesis of the P*n* particles consists of two steps. In the first step, platinum nanoparticles are synthesized via thermal decomposition. It can be shown that by the addition of iron and cobalt doping atoms during the platinum cube formation, cubic particles with an average diameter of 6 nm and narrow size distribution are obtained instead of non-uniform nanodendrites. [1] Compared to pure Pt, the crystal lattice spacing is increased, opening the pathway for heteroepitaxial growth of CFO on the corners of the platinum cubes as shown in Fig. 1.

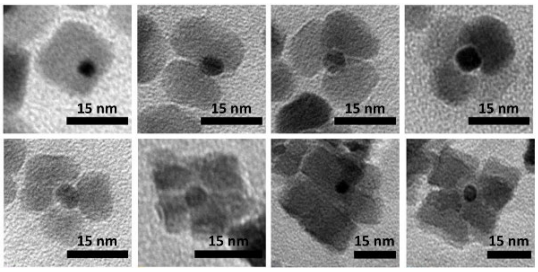

Fig. 1: TEM images of Pt@[$CoFe_2O_4$]$_n$ nanoparticles with n = 1 to n = 8 CFO moieties.

The P*n* particles are obtained in the second synthesis step, in which the platinum cubes are used as seeds for the growth of CFO nanostructures. Depending on the choice of reaction parameters, the number, size, and cubicity of the CFO cubes per nanoobject can be tailored.
In particular, the number of CFO moieties per nanoobject depends on the composition of the reaction mixture with respect to the amphiphiles present. With increasing oleylamine and oleic acid concentration, more CFO surface can be stabilized and therefore more CFO moieties grow per Pt seed. And finally, the *n* of the P*n* particles can be adjusted via the ratio of the CFO precursors to the platinum nuclei in the reaction mixture. With increasing ratio more CFO moieties are obtained.
The nanoobjects are originally dispersed in organic medium and can be transferred to an aqueous phase via a ligand exchange method, resulting in hybrid nanoobjects with excellent diffusion properties, showing experimentally observed hydrodynamic diameters of the equivalent sphere between 20 nm and 35 nm by ACS (rotational) and DLS (transversal).

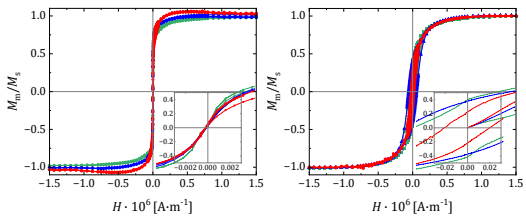

Fig. 2: Normalized field-dependent magnetization curves of P1 (green), P3 (blue), and P8 (red) measured at 298.2 K for dispersion state in water (left) and dried powder (right).

To understand the interplay between the individual substructures in the nanoobjects, we investigate the catalytic and plasmonic properties of the structures on the one hand and perform detailed magnetic investigations on the other. While they show mainly pseudo-superparamagnetic properties in dispersion, powder experiments reveal the predominant magnetically blocked state of the domains (Fig. 2). Differences in the individual

structures are identified and investigated in more detail (see abstract of Joachim Landers, UDE).

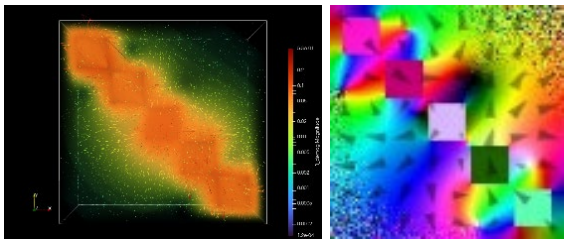

Fig. 3: Micromagnetic simulations of demagnetization fields (left) and magnetization fields (right) of CFO cubes without an external magnetic.

To allow a deeper understanding of the internal magnetization of the hybrid nanoobjects, micromagnetic simulations (*Mumax3*) reveal the magnetic ground state (Fig. 3) and field-induced magnetization of different particle arrangements. By comparison with experimental results, we obtain detailed information on the interaction of magnetic cubes in their geometric environment.

Conclusion

Our results demonstrate the successful synthesis of different morphologies of P*n* particles with predicted composition and geometry. The nanoobjects are characterized in terms of their dynamic, catalytic, plasmonic and magnetic properties, while micromagnetic simulations allow a better understanding of their nanoscale interaction.

Acknowledgements

Financial support by the German Research Foundation (DFG) within project SCHM1747/16-1 is gratefully acknowledged.

References

[1] C. Wang, H. Daimon, T. Onodera, T. Koda, S. Sun, *Angew. Chem*. **120**, 3644–3647 (2008).

Scrutinizing magnetic fields of dipole clusters

I. Rehberg[1], P. Blümler[2], E. Aderhold[3], Th. Friedrich[3]

[1] *Institute of Physics, University of Bayreuth*
[2] *Institute of Physics, Johannes Gutenberg-Universität Mainz*
[3] *Fraunhofer IMTE, Fraunhofer Research Institution for Individualized and Cell-Based Medical Engineering, Lübeck*

Introduction

The particles in magnetic fluids tend to form magnetic clusters, e.g., in the aging process. Macroscopic models in the form of spherical magnets, and computer animations as presented here, mimic the dipole-dipole interaction of the particles and are thus useful tools for understanding the characteristics of such dipole clusters.

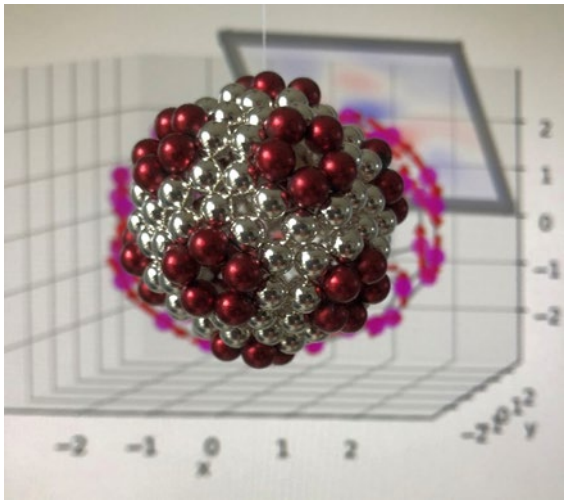

Figure 1. Dipole cluster build from magnetic spheres. The background is a screenshot from Ref. [1].

The app advertised here allows the interactive exploration of more than 500 arrangements of dipoles [1], including:

- Platonic & Archimedean solids,
- simple cubic, FCC & HCP packings,
- 3d-cuts of a tetraplex,
- several stacks of rings.

Figure 2. A dipole cluster from 5 mm neodymium spheres with dodecahedral symmetry. The magnetic order of the dipole orientation will in general reduce that symmetry to a subgroup, which can be interactively explored [1].

The clusters can be scrutinized concerning their

- dipole arrangement & field,
- binding energy & mutual force.

Moreover, the app helps to design tailored magnetic fields from permanent magnets – dipoles and rods – useful for the external manipulation of magnetic fluids [2].

Methods

The app comes as an open source Python script, and as an executable file [1]. For the demonstration experiments, spherical neodymium magnets proofed to be almost perfect dipoles [3].

Results for dipole rings

The ring configuration [4] might be the most prominent for the coagulation of magnetic particles. It is the energetically favored cluster of N dipoles, if $3 < N < 14$ [5]. For larger particle numbers, a tube – formed by a stack of S rings from L dipoles each – is more stable. The field $B(r)$ within these tubes increases with the distance r according to

$$B(r) \sim r^{L-1+\mathrm{mod}(S+1,2)}. \qquad (1)$$

The field decreases far from the tube as

$$B(r) \sim r^{-L-2-\mathrm{mod}(S+1,2)}. \qquad (2)$$

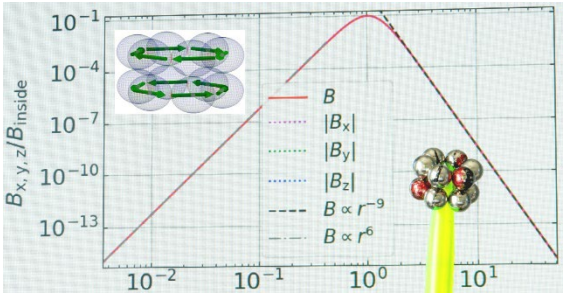

Figure 3. B vs. r, where r is the distance from the centre. The field inside a stack of 2 rings from 6 dipoles each increases with a power of 6, and decreases with a power of -9 outside the arrangement

The force between such tubes decays with

$$F(r) \sim r^{2L-2(1+\mathrm{mod}(S+1,\ 2))}. \qquad (3)$$

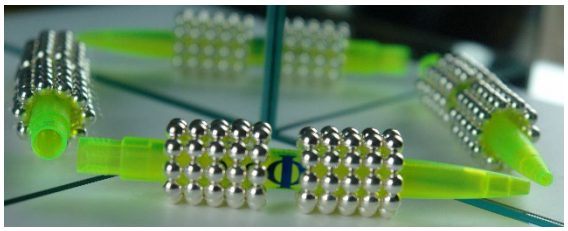

Figure 4. The force between these two S=5 stacks of L=10 rings decreases with a power of -22.

General Result for all dipole clusters

The sum of the powers for the field increase in the center of the cluster and the decrease in the far field is a universal number, namely -3.

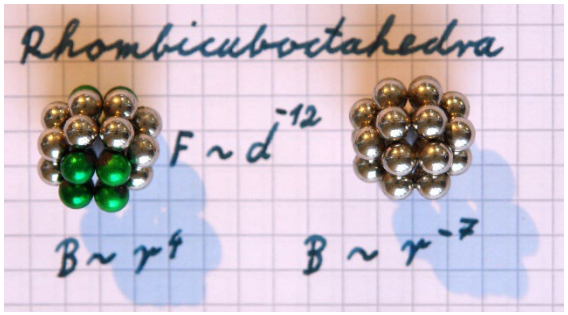

Figure 5. The field in a rhombicubeoctahedron increases with a power of 4 inside and decreases with a power of -7 on its outside, fulfilling the -3-rule. The force between two such clusters decays with -12th power of the distance [1].

Result for Halbach rings

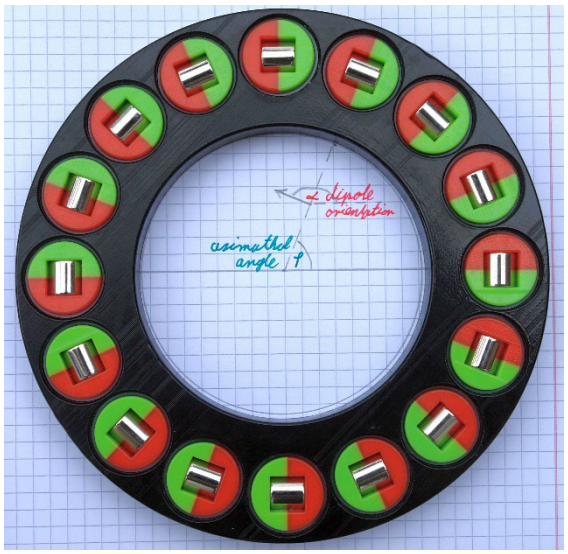

Figure 6: 16 neodymium 1 cm × 1 cm cylinders in red-green coloured holders, which glide on ball bearings and are thus free to rotate. The photo shows the ground state with $\alpha = \varphi + 90°$.

Special arrangements of the permanent magnets along a ring yield an almost homogenous field inside the ring, which is desirable for applications [2]. A dipole orientation $\alpha = 2\varphi$, as originally introduced by Halbach for magnetic rods [6], yields a fairly homogenous field [7], even for the cylindrical magnets shown here. A slight modification of this arrangement, namely

$$\tan\alpha = \frac{3\sin(2\varphi)}{6\cos^2\varphi - 2}, \qquad (4)$$

increases the field strength by about 5%. The area of sufficiently constant field (see V1.2.1 of [1]) enlarges by about 40%.

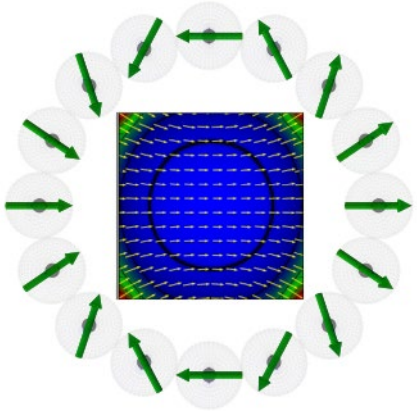

.

Figure 7. A calculation of the magnetic field within the dipole arrangement of eq. (4) using the animation app [1].

Acknowledgments

It is a pleasure to thank Günter Auernhammer, Boyd Edwards, Kyongwan Kim, Jan Lellmann, Andreas Menzel, René Messina, Ivan Novikau, Johannes Schönke, Matthias Schröter, and Igor Stancović for encouraging comments.

References

[1] Rehberg, I. (2024). Does a Magnetic Soccer Ball Carry Toroidal Moment? – An App to Examine 551 Dipole Clusters (2.0). Zenodo. https://doi.org/10.5281/zenodo.12656187.

[2] Blümler, P. (2021). Magnetic Guiding with Permanent Magnets: Concept, Realization and Applications to Nanoparticles and Cells. Cells 10, 2708. https://doi.org/10.3390/cells10102708

[3] Hartung, S., et al. (2018). Assembly of eight spherical magnets into a dotriacontapole configuration, Physical Review B 98, 214424.

[4] Rehberg, I. (2024). Magnetic Tubes – Instability of a Drug Deliverer (Version 1.0.2). Zenodo.

[5] Messina, R., Khalil, L. A., Stanković, I. (2014). Self-assembly of magnetic balls: From chains to tubes. Phys. Rev. E 89, 011202(R).

[6] Halbach, K. (1980). Design of permanent multipole magnets with oriented rare earth cobalt material. Nucl. Inst. Methods 169, 1–10.

[7] Soares, Y.B., et al. (2022). High gradient nested Halbach system for steering magnetic particles. Int J Part Imag 8, 2203012.

Vibration-driven planar motion system based on multipole magnetoactive elastomers

M. Reiche[1], L. Zentner[1], D. Borin[2], T.I. Becker[1]

[1] *Mechanics of Compliant Systems Group, Faculty of Mechanical Engineering, Technische Universität Ilmenau, 98684 Ilmenau, Germany*
[2] *Magnetofluiddynamics, Measuring and Automation Technology, Technische Universität Dresden, 01062 Dresden, Germany*

Magnetoactive elastomers (MAEs) consist of an elastic matrix containing micron-sized magnetically soft and/or hard particles. These intelligent materials can change their material properties under the influence of external or internal magnetic fields. Of particular interest are MAEs with hard magnetic particles that act as elastic permanent magnets after magnetization in a strong magnetic field [1,2].
Motion systems realized with MAEs can be driven with a minimum number of actuators. This work focuses on the development of locomotion systems based on multipole MAEs that achieve planar locomotion through field-induced vibrations of MAE elements, that contain both hard and soft magnetic particles (Fig. 1).

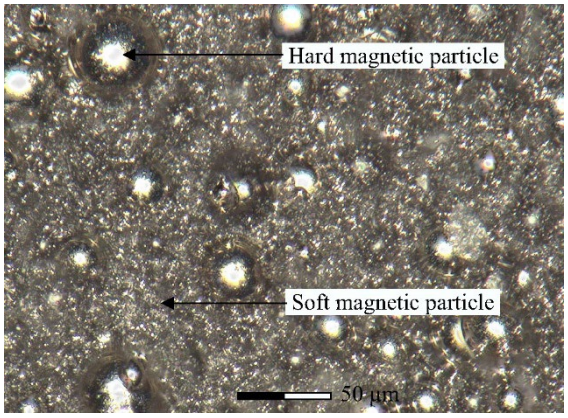

Figure 1. Microscope image of the MAE surface filled with magnetically hard and soft particles.

Two MAE beams are magnetized in a strong magnetic field so, that they have a north pole at each end and a south pole in the middle. A layer of silicone bristles is glued to the underside of each MAE beam and above each beam, there is an electromagnetic coil supplied with a square wave voltage. The attracting and repelling magnetic forces induce periodic bending vibrations of the MAE beam. In combination with asymmetrical friction forces caused by angled silicone bristles, these transverse vibrations result in a shift of the horizontal position during each oscillation cycle. The previously developed system with one MAE beam based on this type of actuation shows one-directional motion with a maximum advancing velocity reached in the resonance frequency range [3].
The planar locomotion system incorporates two multipole MAE beams, which are arranged parallel to each other through a mounting and actuated by two coils (Fig. 2). The velocity and direction of movement are controlled by selecting the coils actuating frequencies. Different actuating frequencies of the MAE beams generate the side steering effect. The velocity shows a strong resonance dependency on the excitation frequencies. Velocities of over 100 mm/s are achieved in the resonance range around 60 Hz (Fig. 3).
Investigating the system's side steering behavior demonstrate the motion controllability within the plane. Figure 4 shows the motion trajectories for a fixed actuation frequency of the left coil at f_L =80 Hz and a variable frequency of the right coil f_R. Depending on the frequency ratio, straight or curved movement can be enabled. For curved movement high yaw rates are achieved, with the maximum yaw rate occurring during a left turn trajectory when the right coil actuation frequency is f_R =55 Hz. These movement characteristics make the system suitable for use in complex environments.
The use of multipole magnetized MAEs enables the realization of both, direction and velocity controllable locomotion systems with a minimal number of actuators. In future work, the scaling potential can be explored, along with the implementation of autonomous energy supply.

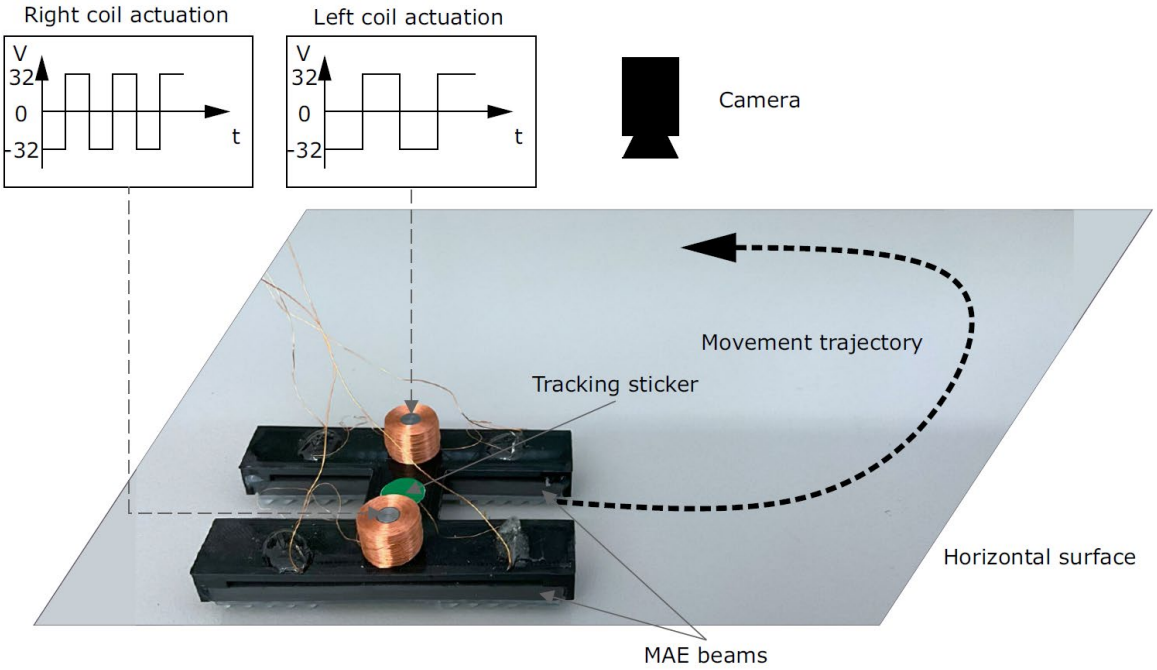

Figure 2. Planar locomotion system with schematic illustration of the motion capture measurement setup.

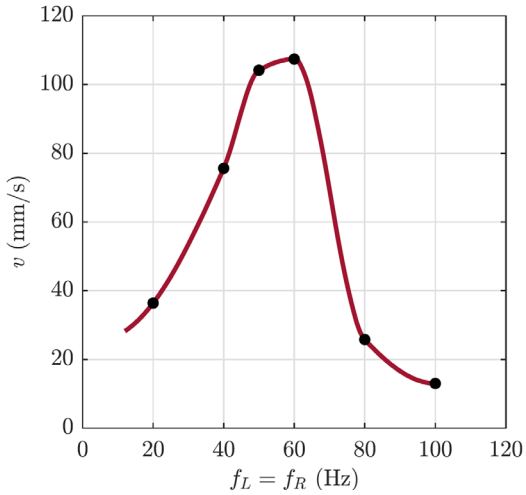

Figure 3. Advancing velocity at equal excitation frequencies of the left and right coils.

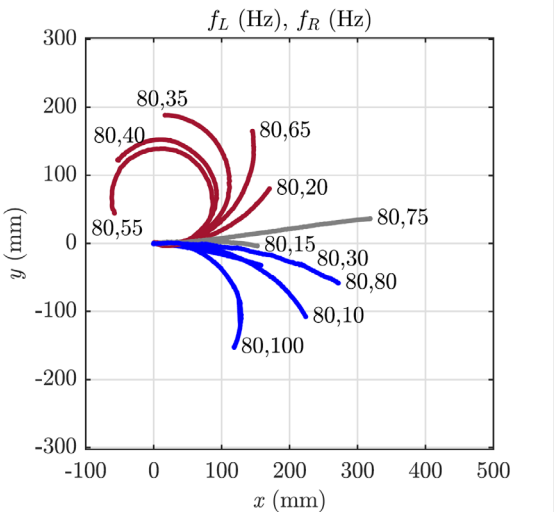

Figure 4. Motion trajectories for a fixed left coil frequency of f_L = 80 Hz and various right coil frequencies f_R.

Acknowledgments

The work is funded by the Deutsche Forschungsgemeinschaft (DFG), project BE-6553/2-1.

References

[1] T.I. Becker, O.V. Stolbov, D.Yu. Borin, K. Zimmermann, and Yu.L. Raikher. Basic magnetic properties of magnetoactive elastomers of mixed content. Smart Materials and Structures 29 (2020) 075034.

[2] T.I. Becker, O.V. Stolbov, A.M. Biller, D.Yu. Borin, O.S. Stolbova, K. Zimmermann, Yu. L. Raikher. Shape-programmable cantilever made of a magnetoactive elastomer of mixed content. Smart Materials and Structures 31 (2022) 105021.

[3] M. Reiche, T.I. Becker, G.V. Stepanov, K. Zimmermann. A multipole magnetoactive elastomer for vibration-driven locomotion. Soft Robotics 10(4) (2023) pp. 770-784.

The role of shape anisotropy of hematite nanodopants in ferronematic liquids

G. Richwien,[1] B. Rhein,[1] J. Kopp,[2] H. Nádasi,[3] A. Eremin,[3] J. Landers,[1] A. M. Schmidt[2]

[1] *Department for Chemistry and Biochemistry, University of Cologne*
[2] *Faculty of Physics and Center for Nanointegration Duisburg-Essen (CENIDE), University of Duisburg-Essen*
[3] *Institute of Physics, Otto von Guericke University Magdeburg*

Controlling the director in thermotropic liquid crystals (LC) by means of external fields is a powerful tool in a wide range of applications, e.g., in optical devices. Usually, such devices are operated by electric voltage, while an analogous employment of magnetic fields is principally an option, yet drawn back by the need for high magnetic flux density due to the low magnetic anisotropy of the mesogenic molecules.

In order to increase the effect of magnetic fields on liquid crystal phases, it has been proposed to use fine magnetic particles as dopants and has ever since inspired a number of experimental approaches toward such magnetically doped liquid crystal phases. Our tactic towards ferromagnetically doped LCs with enhanced volume fraction and stability of the magnetic dopants is based on a general approach to surface-modify magnetic nanoparticles with a side-chain LC polymer brush. We employ two different synthetic pathways with a variation of shell thickness, mesogen density and spacer length. This results in an effective steric stabilization of the particles against agglomeration and offers a high degree of surface density with respect to the mesogen.

Spindle-like hematite nanoparticles are created in a hydrothermal decomposition of $FeCl_3$ in water in the presence of NaH_2PO_4. It is confirmed that the concentration of hydrogen phosphate influences the aspect ratio of the hematite nanoparticles by TEM, DLS and ACS experiments, revealing that the shape of the particles can be varied between elongated spindles ($p \sim 5$) and cubic ($p = 1$). The crystalline structure of the hematite nanoparticles is confirmed for all the investigated nanoobject batches. A Morin transition is not observed for nanoobjects with $p > 1.5$ (see abstract contribution of J. Kopp), and both coercivity and the normalized remanent magnetization increase with increasing aspect ratio.

We carefully investigate the phase behavior of 5CB when doped with different, appropriately surface-modified hematite nanoobjects, divergent in size, shape and magnetic anisotropy, and under variation of the particle volume fraction.

Our results from differential scanning calorimetry (DSC), refractometry and polarized optical microscopy provide insight into the impact of the aspect ratio on the stability and the ferronematic coupling properties. The magnetic response of the ferronematic phases is investigated by capacitance measurements in a magnetic field. As compared to 5CB, the critical magnetic field strength is shifted to significantly lower fields.

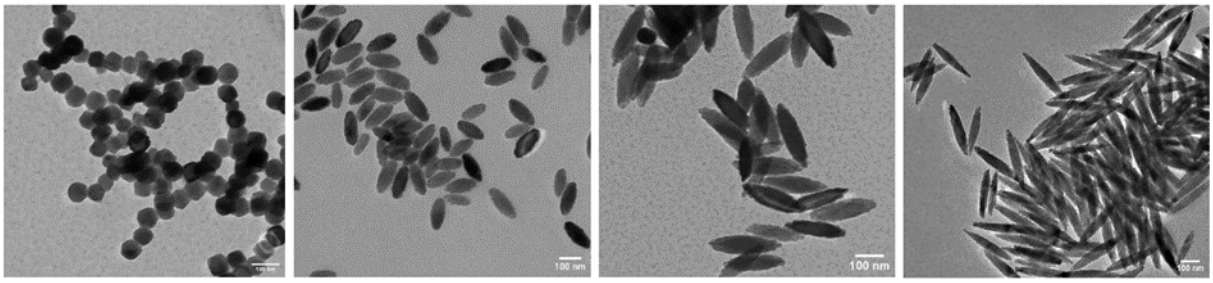

Figure 4.1. TEM images of spindle-like hematite nanoparticles with varying aspect ratio prepared at different synthetic conditions. Left to right: p = 1.0; p = 2.5; p = 3.8; p = 5.2.

With increasing aspect ratio of the dopants, the effect on the magnetic Fréedericksz transition is stronger.

Acknowledgments

We acknowledge support of this study by the DFG (projects SCHM1747/16-1, LA5175/1-1 and NA1668/1-3)!

References

[1] M Ozaki, S Kratohvil, E Matijevic; **J. Colloid Interf. Sci. 102**, 146-151 (1984)
[2] K Koch, M Kundt, A Barkane, H Nadasi, S Webers, J Landers, H Wende, A Eremin, AM Schmidt; **Phys. Chem. Chem. Phys. 23**, 24557-24569 (2021)
[3] K Koch, M Kundt, A Eremin, H Nadasi, AM Schmidt; **Phys. Chem. Chem. Phys. 22**; 2087 - 2097 (2020)

Towards an effective material model for magneto-active elastomers

D. Romeis, M. Roghani, M. Saphiannikova

Leibniz-Institut für Polymerforschung Dresden e.V., Hohe Straße 6, 01069 Dresden

The theoretical modeling of magneto-active elastomers (MAEs) represents a very challenging task until today. The difficulties arise from many complex and intertwined responses on the micro to the macro scale. In absence of magnetic field the material is typically described in terms of a rubber reinforced by hard filler particles. Yet, when an external magnetic field is applied, the situation drastically changes. Due to the softness of the elastomeric matrix, the activated magnetic interactions among the particles cause them to move and to induce deformations of the embedding elastomer. The long-range nature of these interactions results in macroscopic deformation of the sample and in microscopic reallocation of the particles, typically clustering into chain-like structures along the applied field direction. Due to the varying shape and particle distribution in the composite, also a constantly changing magnetization behavior is generated. These effects are magnetically and mechanically strongly coupled.

A prominent approach to characterize this material is the homogenization of micro-continuum simulations. Yet, the manifold of parameters to be analyzed in such detailed simulations makes the procedure quite elaborate. Such models are usually based on the Finite Element Method and can not describe large deformation processes and subsequent clustering of hard filler particles.

In this talk we want to present an alternative formalism [1] where the magnetic part is homogenized with the help of the dipolar mean-field approach [2] and the mechanical contribution is considered using a modified transversely isotropic Neo-Hookean material model. The resulting equations contain only a small number of meaningful parameters. Our unified mean-field model is adapted to an experimental setup measuring a large magneto-deformation of cylindrical MAE samples. Using the material parameters as obtained from experimental measurements for the samples in absence of a magnetic field, we find very good agreement to the observed magneto-deformations in applied fields [3]. Additionally, we can predict the changes in the magnetization behavior due to microstructure evolution, i.e., clustering into dense columns along an applied field. It is found, that our model is able to describe the effective magnetization curves observed in corresponding experiments. This shows that the unified mean-field model provides quantitative access to essential material properties in MAE samples with different shapes and evolving particle arrangements.

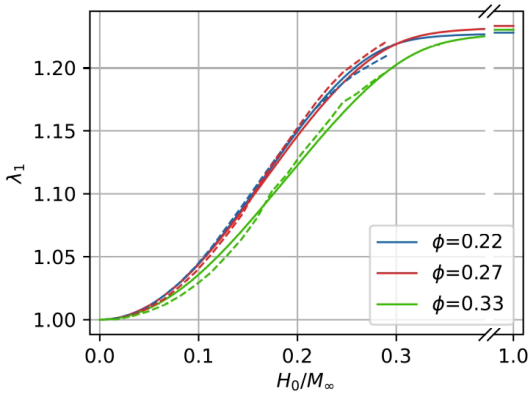

Acknowledgments

Financial support by German Research Foundation (DFG) via research project 380321452/GRK2430 is gratefully acknowledged.

References

[1] M. Roghani, D. Romeis, M. Saphiannikova. Effect of microstructure evolution on the mechanical behavior of magneto-active composites. Soft Matter **19**: 6387 (2023).

[2] D. Romeis, M. Saphiannikova. Effective magnetic susceptibility in magnetoactive composites. J. Magn. Magn. Mat. **565**: 170197 (2023).

[3] M. Roghani, et.al. Magnetically induced deformation of isotropic magneto-active elastomers and its relation to the magnetorheologi-

cal effect. Submitted to Composites Part B (2024).

Hydrogels Based on Magnetoplasmonic Nanoparticles in a Thermo-Responsive Polymer Matrix

P Schütz[1], S. Lemich[1], M. Weißpflog[1], P. Körner[1], V. Abetz[1,2*], and B. Hankiewicz[1]
[1] *Institut für Physikalische Chemie, Universität-Hamburg, Grindelallee 117, 20146 Hamburg, Germany.*
[2] *Institute of Membrane Research, Helmholtz-Zentrum Hereon, Max-Planck-Straße 1, 21502 Geesthacht, Germany.*

Optimized nanomaterials for biomedical applications like targeted drug delivery or hyperthermia need to fulfill multiple functions, e.g., enabling biocompatibility, targeting specific areas, producing heat, or releasing a substance as a response to an external stimulus. Magnetoplasmonic nanoparticles (MNPs), which are a hybrid material based on a magnetic NP core and a plasmonic gold shell, are interesting platforms for these multi-responsive materials.[1] Due to the magnetic core, the MNPs can be moved using magnetic fields, while the gold shell adds optical properties and chemical stability to the system. The abovementioned properties make MNPs an interesting alternative to magnetic NPs or gold NPs and open up different applications utilizing the properties of both components.[2] Besides the MNP system, the ligands or matrix in which they are embedded are an essential factor in creating optimized materials since they cannot only stabilize the MNPs but can also be utilized to add more functionalities to the system. Polymers can be used as versatile matrix materials to create both microspheres or solid bulk materials for different biomedical and technical applications.

In this work, we present a novel synthesis route to obtain multi-responsive hydrogels, which are based on MNPs in a thermo-responsive polymer matrix, as shown in Figure 1. The MNPs are based on $CoFe_2O_4$-NPs (CF-NPs) as magnetic cores, which were encapsulated with gold. The synthesis of the MNPs was performed in an aqueous medium using the amino acid L-cysteine as a non-toxic ligand.

The MNPs were then functionalized with a double thermo-responsive *graft*-copolymer consisting of a poly[oligo(ethylene glycol) methacrylate] backbone and multiple poly(*N*-isopropyl acrylamide) side chains.[3] Due to the used synthesis method, each polymer chain was terminated with trithiocarbonate groups, which could be anchored to the gold surface of the MNPs. These CF@Au@Polymer-MNPs were characterized regarding their magnetic, optical, and thermo-responsive properties to demonstrate that the properties of each component were present in the hybrid material.

Finally, the CF@Au@Polymer-MNPs were crosslinked to obtain hydrogels that show temperature-dependent swelling behavior. Using NIR irradiation, this thermo-responsive behavior can be utilized to trigger the deswelling of the hydrogel and to allow a controlled release of a substance dispersed in the water phase.

Acknowledgments

The authors would like to thank the Deutsche Forschungsgemeinschaft for funding this project within the RTG 2536.

References

[1] M. Lázaro, P. Lupiáñez, J. L. Arias, M. P. Carrasco-Jiménez, Á. V. Delgado, G. R. Iglesias, *Polymers* **2022**, *14*.
[2] G. J. Yoon, S. Y. Lee, S. B. Lee, G. Y. Park, J. H. Choi, *Nanomaterials* **2018**, *8*.
[3] J. Xu, V. Abetz, *Soft Matter* **2022**, *18*, 2082.

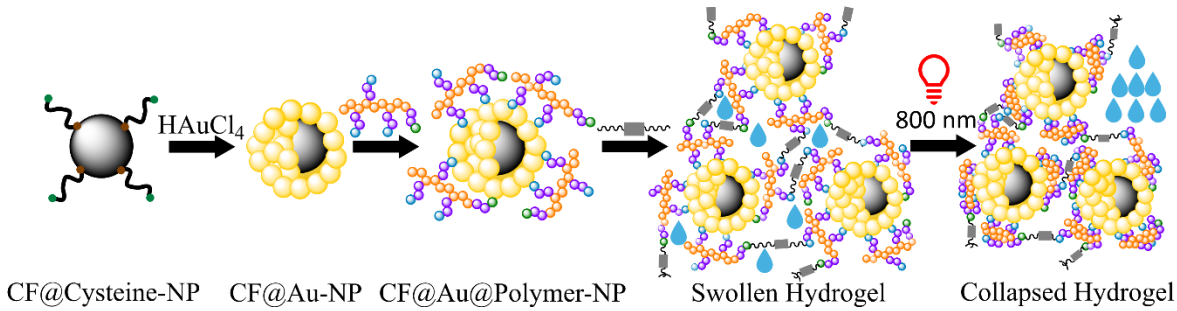

Figure 1: Schematic of the synthesis route of the multi-responsive hydrogel and the swelling behavior of the hydrogel which can be remotely triggered using NIR irradiation. The synthesis route starts from L-cysteine functionalized CF-NPs, which are encapsulated in gold, functionalized with polymers, and crosslinked to obtain the hydrogel.

Studying the nanoparticle-polymer interaction in magnetic gels using computer simulations

R. Stephan, C. Pabshettiwar, C. Holm and R. Weeber

Institut für Computerphysik, Universität Stuttgart, Allmandring 3, 70569 Stuttgart, Germany

Introduction

Magnetic gels are of interest, as one can control their shape, viscoelastic properties and motion by means of an external magnetic field. This gives rise to various potential applications, e.g. in biomedicine. Both, the structure of the polymer network, and its coupling mechanisms to the embedded magnetic nanoparticles (MNPs) strongly influence the gel's response to magnetic fields. In our contribution, we focus on the coupling between the polymers and the magnetic nanoparticles. Typically, Van der Waals forces, hydrogen bonds or electrostatic interactions trap the MNPs within the polymer network. Moreover, functionalized MNPs can act as cross-linkers to form a hybrid network with the polymers. Additionally, the polymers and magnetic nanoparticles interact hydrodynamically by means of the solvent. It has been shown [1,2] for MNPs in polymer solutions that a hydrodynamic coupling alone is sufficient to capture experimentally observed trends in AC susceptibility spectra [3].
In this contribution, we investigate how different MNP-polymer interactions affect the dynamic magnetic properties of the gel. To this end, we set up a computer simulation of a magnetic gel with interchangeable MNP-polymer interactions. From these we obtain both, magnetic susceptibility spectra and structural details of the microscopic environments of the magnetic nanoparticles.

Simulation model

Our system consists of mainly three parts: the polymer network, the embedded MNP and the fluid. We use the ESPResSo software for molecular dynamics simulations of soft matter to simulate a coarse-grained system [4]. The polymers are implemented using the bead-spring formalism. One bead in the simulation represents several monomers. Polymer chains in their stretched state are cross-linked into a tetrafunctional network and relaxed into their natural coiled state. The fluid is modelled using the Lattice-Boltzmann algorithm. We assume that the MNPs are magnetically blocked and reorient their magnetic moment by a rotation of the particle as a whole. The MNP is constructed using the so-called raspberry model to couple its rotation to the lattice-Boltzmann fluid. These additional coupling points, however, do not affect the MNP-polymer interaction. In our simulations, we use a single MNP in its polymer environment, representing a situation with very low MNP concentration in experiments. A visualization of the model can be found in Figure 1.

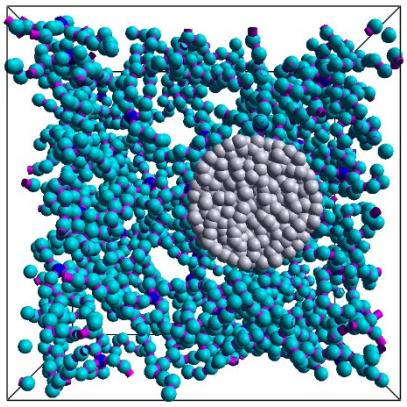

Figure 1: Snapshot of the simulated magnetic gel with polymer network (blue) and MNP (grey).

MNP-polymer interactions

In the simplest case, a purely repulsive potential between the polymer beads and the MNP center ensures excluded volume of the particles without any attraction. In the next step, we use attractive spherical-symmetric potentials with different well widths. In both cases solely hydrodynamic interactions transfer between the rotation of the MNP and the polymer network. Finally, we introduce specific attractive sites on the surface of the MNP adding a direct coupling between the polymer network and the rotation of the MNP. The polymer beads are not bound covalently

to the MNP surface but rather experience an attractive force in proximity of these sites mimicking a surface roughness of the MNP.

Results

We study the magnetic behavior for the different MNP-polymer interactions dependent on the mesh size of the polymer network. Even for a purely repulsive interaction between MNP and polymers, we observe a clear shift of the susceptibility spectra towards lower frequencies for smaller mesh sizes. This corresponds to higher Brownian relaxation times. For a spherically symmetric attractive MNP-polymer interaction, this shift is significantly higher. We relate this to a higher polymer density close to the surface of the MNP, and thus stronger hydrodynamic coupling between the orientation of the MNP and the polymers.

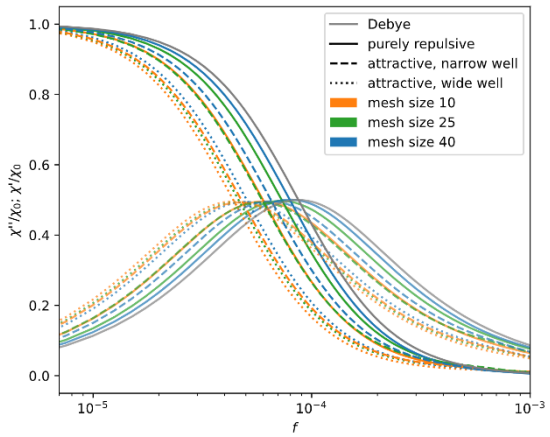

Figure 2: Magnetic susceptibility spectra for various spherically symmetric MNP-polymer interactions dependent on mesh size of the polymer network. We can see a shift towards lower frequencies for decreasing mesh widths as well as for the attractive interactions.

We now break the spherical symmetry of the MNP-polymer interaction by introducing attractive coupling sites on the surface of the MNP. Here, we observe polymer beads directly docking to the MNP surface at these sites. This adds an additional coupling be-tween the MNP's orientation and the polymers. Depending on the strength of the attraction, the magnetization behavior of the gel changes significantly. For lower attraction strengths, the docking of the polymers to the sites is reversible and a Langevin-like magnetization response is maintained. For a stronger attraction on the other hand, we observe hysteresis, as the polymer beads hold the MNP in place and hinder its rotation. In summary, for spherically symmetric MNP-polymer interactions, the MNP orientation couples to the polymers via hydrodynamics. This coupling is stronger, when the polymers are closer to the MNP surface. By breaking spherical symmetry in the MNP-Polymer interaction an additional coupling is introduced and the gel's magnetization response is significantly different.

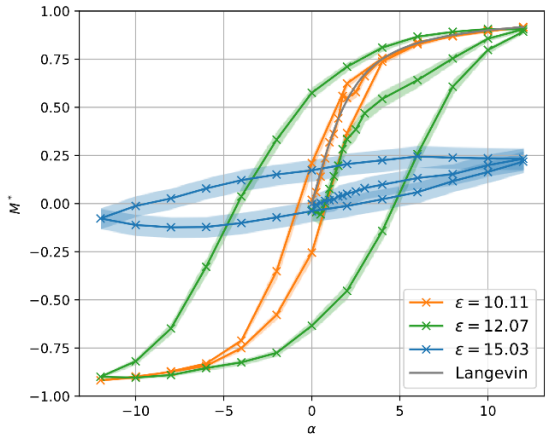

Figure 3: Static magnetization curve with hysteresis for MNP-polymer coupling via attractive sites on the MNP surface dependent on the depth of the attractive potentials.

Acknowledgments

The authors acknowledge support by the state of Baden-Württemberg through bwHPC and the German Research Foundation (DFG) through grant INST 35/1597-1 FUGG.
RW and CH acknowledge support through the Cluster of Excellence EXC 2075 SimTech, funded by the German Science Foundation, grant no. 390740016.

References

[1] P. Kreissl, C. Holm and R. Weeber. *Frequency-dependent magnetic susceptibility of magnetic nanoparticles in a polymer solution: a simulation study.* Soft Matter, 17(1), (174-183), 2021.

[2] P. Kreissl, C. Holm and R. Weeber. *Interplay between steric and hydrodynamic interactions for ellipsoidal magnetic nanoparticles in a polymer suspension.* Soft Matter, 19(6), (1186-1193), 2023.

[3] E. Roeben, L. Roeder, S. Teusch et. al. *Magnetic particle nanorheology*. Colloid and Polymer Science 292, (2013–2023), 2014.

[4] F. Weik, R. Weeber, K. Szuttor et. al. *ESPResSo 4.0 – an extensible software package for simulating soft matter systems*. The European Physical Journal Special Topics 227(14), (1789–1816), 2019.

Influence of light irradiation on Iron Oxide Nanoparticles

A. Weidner[1], D. Eberbeck[2], S. Dutz[3,4]

[1] *Fachgebiet Elektrochemie und Galvanotechnik, Technische Universität Ilmenau, Germany*
[2] *Physikalisch-Technische Bundesanstalt, Berlin, Germany*
[3] *Leupold Institute for Applied Natural Sciences (LIAN), Westsächsische Hochschule Zwickau, Germany*
[4] *Institut für Biomedizinische Technik und Informatik (BMTI), Technische Universität Ilmenau, Germany*

Introduction

Nanoparticles based on iron oxides (IONP) are interesting materials due to their easy availability, low cost and good biocompatibility combined with usable magnetic properties. In recent years many applications e.g., in biomedicine (imaging (MPI, MRI), magnetic hyperthermia, targeted drug delivery) or industry (waste water treatment) were developed. While emphasis was put on investigating and tuning magnetic properties also optical properties came into focus within the last years [1,2]. As many iron oxides in bulk are semi-conductors and IONP-suspensions show high absorption rates in the visible light spectrum, photothermal and photoelectrical properties could be interesting e.g., for applications in photohyperthermia or catalysis. Additionally, questions arise concerning storage and sterilization of IONP (esp. UV-sterilization) and characterization techniques based on the interaction with light.
Therefore, the aim of this research is to investigate the influence of irradiation with a high intensity light source in the visible light range on different IONP-suspensions with special focus on colloidal stability and heating effects.

Preparation and characterization

For first experiments IONP were prepared by co-precipitation of iron salt solutions ($FeCl_2$ / $FeCl_3$) by adding 1 M $NaHCO_3$ solution at 50 °C under permanent stirring at a flow rate of 1.2 ml/min, followed by boiling to remove CO_2 and form iron oxide multicore nanoparticles (MCNP). These MCNP have been coated with adsorptive shells featuring different stabilizing mechanisms and surface charges: citric acid (CA) and carboxymethyl dextran (CMD) - both electrostatic, negative; diethylaminoethyl-dextran (DEAE) - electrostatic, positive; starch (St) - steric.
Three samples (V = 3 ml; β ~ 1 g/l) were filled each in borosilicate glass vessels and 1) irradiated for 1h (1hL) with a high intensity white light LED (100 W Oumurui, Genesis 30MIL chip, 6,25 cm², 6000 - 6500 K, 8000 – 9000 lm; run at 60 W) with a glass lens (h = 1.9 cm; d = 4 cm) at a distance of 4.2 cm from the LED, 2) kept at 75 °C in an oil bath for 1h (1h 75 °C) and 3) kept without any treatment (noL). The temperature for 1hL-samples was recorded with a fiber optic temperature sensor. The resulting IONP were analyzed by UV-VIS-measurements to determine the absorption behavior and dynamic / electrophoretic light scattering (DLS / ELS) to determine size distribution and surface charge.
In a second step commercial IONP were investigated by filling each of 3 ACS-vials (borosilicate glass) with 100 µl of IONP-suspension (β ~ 0.1 g/l). These samples were 1) irradiated 1h with the same light source (1hL) or 2) heated 1h at 75 °C (1h 75°C) in a water bath. One vial was kept as reference 3) (noL). The treated samples were investigated by DLS / ELS as well as with AC-susceptometry (ACS) as magnetic method to avoid interactions with light.

Results and discussion

Photothermal properties: The irradiation with the intense light led for all MCNP-suspensions to an increase in temperature within 10 - 15 min. Temperatures up to 86 °C and heating rates of up to 16 K/min could be observed (see fig.1), what shows the potential for photothermal applications. It can be seen, that the temperature increase is not uniformly, what could be interpreted by the agglomeration of the MCNP and hint at photoelectrical processes using the light energy.

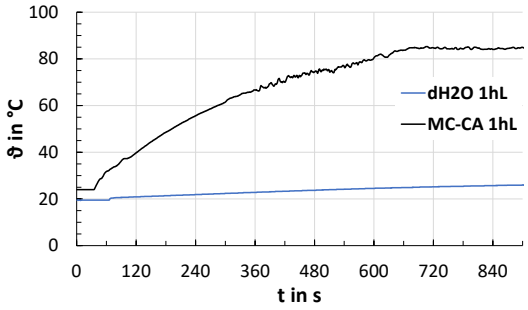

Fig. 1) Exemplary heating curve for irradiation with a white light LED (60 W) measured for CA-MCNP (V = 3 ml, β ~ 1 g/l) and distilled water.
Irradiated MCNP heat the suspension up to ϑ ~ 86 °C with heating rates (25 -> 40 °C) up to 16 K/min.

Influence on IONP-suspension's stability:
Negatively charged CA- and CMD-MCNP agglomerated and fully sedimented during 1h of light exposure. The ζ-potentials shifted from negative values to ζ ~ 0 mV for CMD-MCNP or even positive values (ζ = 27 mV) for CA-MCNP, whereas for the 1h 75°C-MCNP the ζ-potential remained unchanged. DLS-measurements confirmed similar size distributions for 1h 75°C- and noL-samples, but persistent agglomerates for 1hL-samples. This behavior can be interpreted with desorption of the coating by either photothermal conversion of the light and resulting high surface temperatures or photoelectrically by changing the surface charge and weakening adhesion forces. Similar results were found for other negatively coated commercial IONP (e.g., Synomag® (surface: COOH), micromod Partikeltechnologie GmbH Germany), although not all IONP showed this behavior (e.g.: SHP-30 Carboxyl IONP, OCEAN NANOTECH LLC, USA). Interestingly, all IONP showing sedimentation form loose self-organized 3D-structures (see fig. 2) supporting the interpretation with photoelectrical effects.
For positively coated DEAE-MCNP the formation of non-persistent aggregates can be seen during light irradiation, but no sedimentation was visible after the exposure. DLS confirmed the same size distribution for noL-, 1h L- and 1h 75°C-samples. A similar behavior was observed for positively coated commercial IONP (e.g., fluidMAG-DEAE, chemicell, Germany).
Steric stabilized St-MCNP sedimented during 1h of light exposure, but could be resuspended by ultrasound, what was proven by DLS. The ζ-potential changed from -10.7 mV to 14.3 mV, what hints again on a photoelectrical effect.

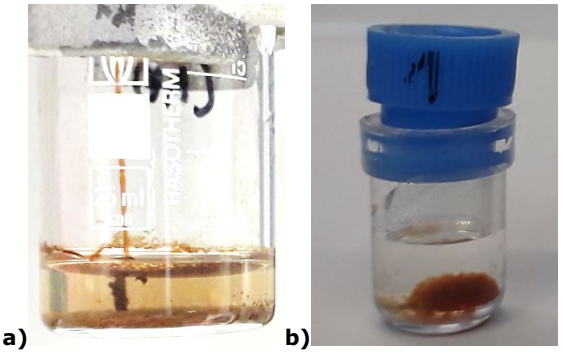

Fig. 2) a) Self-prepared CA-MCNP and **b)** commercial Synomag®-IONP (surface: COOH, micromod Partikeltechnologie GmbH, Germany) after 1h of light irradiation.
The IONP agglomerate and sediment in loose 3D-structures.

Conclusion and outlook

Our study showed, that IONP have a high potential for photothermal applications by reaching temperatures up to 86°C and heating rates of 16 K/min (V = 3 ml; β ~ 1 mg/ml). For several negatively coated IONP a persistent agglomeration and sedimentation in loose self-organized 3D-structures and an increase of surface charge was found, that could be interpreted with the desorption of the coating hinting on photoelectrical effects induced by light. Positively coated IONP did not show changes, whereas sterically stabilized St-IONP show non-persisting agglomeration and a shift to positive surface charges.
Following investigations will focus on understanding the underlaying processes to explain the different behavior found as well as on the kinetics of agglomerate formation during irradiance e.g., by magnetorelaxometry (MRX). Also, dependencies on the wavelength and power of the used light will be addressed, e.g., using laser. Furthermore, magnetic and heating properties of the resulting agglomerates as well as possible applications e.g., for photohyperthermia or flocculation in waste water treatment will be investigated.

References

[1] A. G. Roca et al., Physics Reports **2023**, 1043: 1-35. DOI: 10.1016/j.physrep.2023.10.003
[2] Ximin Cui et al., Chem. Rev. **2023**, 123: 6891-6952. DOI: 10.1021/acs.chemrev.3c00159

Non-Stoichiometric Cobalt Ferrite Nanoparticles by Green Hydrothermal Synthesis and their Potential for Hyperthermia Applications

M. Weißpflog[1*], N. Nguyen[1], N. Sobania[1], and B. Hankiewicz[1*]

[1]*Institute of Physical Chemistry, University of Hamburg, Grindelallee 117, 20146 Hamburg, Germany*
**e-mail of correspondence: maria.weisspflog@gmail.com, birgit.hankiewicz@uni-hamburg.de*

In hyperthermia applications, magnetic nanoparticles (MNPs) characterized by high saturation magnetization and Brownian relaxation dynamics are subjected to an alternating magnetic field, resulting in localized heat generation that targets tumor cell destruction. Among various types of ferrites, magnetite exhibits the highest magnetic moment, contributing to elevated saturation magnetization values. However, iron oxide demonstrates a tendency to oxidize and behaves as a soft magnetic material, leading to relaxation governed by the Néel mechanism for particle diameters up to 20 nm. In contrast, cobalt ferrite nanoparticles (CFNPs) present considerable potential due to their superior magneto-crystalline anisotropy compared to iron oxide, which confers hard magnetic properties. Consequently, the Brownian relaxation mechanism is feasible for CFNPs exceeding 7 nm in diameter. This study is therefore focused on the synthesis of non-stoichiometric CFNPs, wherein reduced concentrations of Co^{2+} ions facilitate high saturation magnetization values alongside the Brownian relaxation mechanism (see **Figure 1A**).[1] Utilizing a two-step synthesis approach that incorporates akaganeite nanorod precursors followed by an aqueous hydrothermal reaction without using toxic surfactants or solvents, we successfully synthesized cubic and spherical $Co_xFe_{3-x}O_4$ nanoparticles with composition

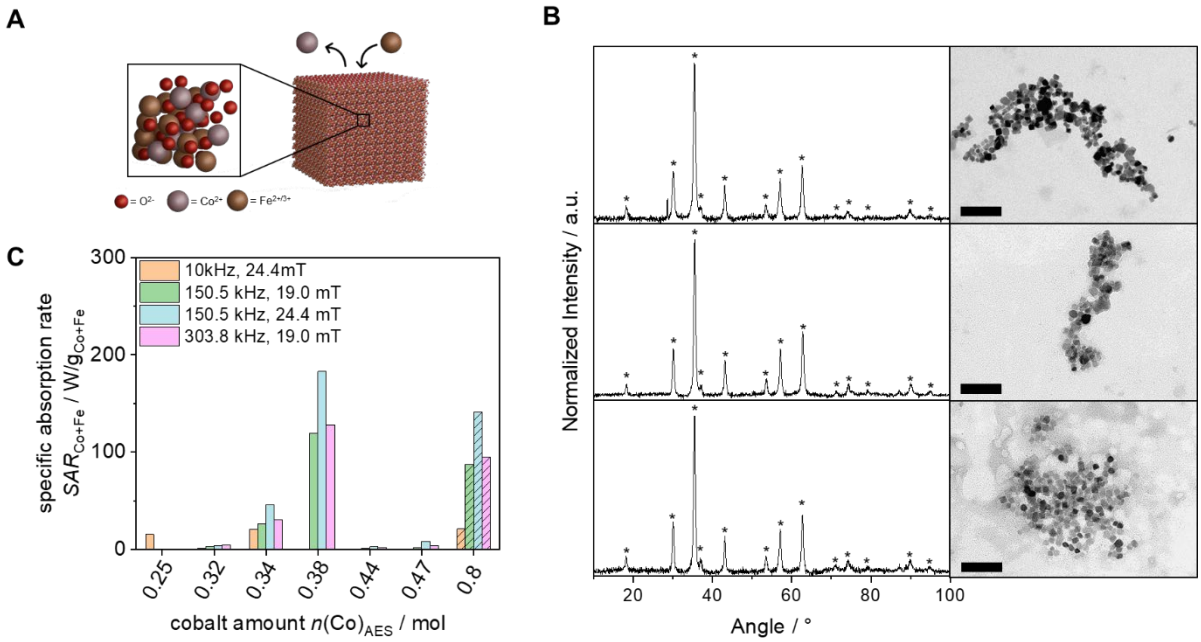

Figure 1. *(**A**) The reduced cobalt ion amount in the crystal structure of cobalt ferrite in a cubic nanoparticle shape will lead to formation of non-stoichiometric CFNPs. **(B)** X-ray diffractograms and TEM images of the non-stoichiometric cobalt ferrite nanoparticles synthesized with a molar ratio of akaganeite to metal salts of 0.5 (top), 1 (middle), and 2 (bottom) at 10 bar. All the observed diffraction reflexes are in good agreement with the cubic spinel structure of $CoFe_2O_4$ (stars, JCPDS no. 00-022-1086). The scale bars show 100 nm for all micrographs. **(C)** SAR values of non-stoichiometric CFNPs are displayed in dependency on the cobalt amount in the crystal lattice. The values of the reference sample[2] synthesized by co-precipitation (x = 0.80) is displayed with lines.*

ranges of $0.25 < x < 0.45$, as illustrated in **Figure 1B**. The saturation magnetization values of up to 75 Am²/kg, are comparable to nearly stoichiometric CFNPs[2] ($x = 0.80$) produced *via* conventional coprecipitation method.

The hyperthermia-induced temperature increase of up to 9.9 K within a 10-minute interval at an excitation frequency of 10 kHz and an applied magnetic field of 24.4 mT holds significant implications for medical applications, including magnetic particle imaging and cancer therapy. By optimizing the excitation parameters, we achieved a temperature elevation of 43 K/10 min at 150.5 kHz and 19.0 mT, while remaining within the biological limits for non-selective heating. The specific absorption rates (*SAR*) ranged from 42 to 58 W/g_{MNP} for lower cobalt concentrations of 50 to 60% in comparison to near-stoichiometric NPs. The *SAR* of the CFNPs in dependeny on the cobalt amount is shown in **Figure 1C**. The *SAR* of NPs with a composition of $x = 0.38$, which attains values up to 183 W/g_{Co+Fe}, is 30% greater than that of near-stoichiometric CFNPs with a composition of $x = 0.80$ synthesized *via* coprecipitation methods. Importantly, the reduction in cobalt content by up to 52% did not negatively impact the hyperthermia performance, thereby enabling a more environmentally sustainable synthesis methodology.

Conclusion and Outlook

In conclusion, this work is of paramount importance for the environmentally benign aqueous synthesis of magnetic CFNPs, as it facilitates a reduction in cobalt content without compromising hyperthermic efficacy or specific absorption rates. Given the prevalent concerns regarding the toxicity of cobalt, the application of cobalt ferrite in hyperthermia treatments has often been limited. In this context, we present non-stoichiometric particles that demonstrate high heating efficiency. Furthermore, as evidenced by previous studies, the cytotoxicity of cobalt ferrite, cobalt-doped magnetite, and magnetite does not exhibit significant differences.

By analyzing this particle system and the underlying mechanisms, these can be utilized for further investigations. Employing a core-shell system, the initiation phase of particle formation will be examined resulting in a pronounced dependency of the magnetic partciles´size and cobalt content on the shell thickness of a core-shell-precursor system.[3] Furthermore, future studies will aim to increase the fraction of shape-anisotropic particles by modifying the Reynolds number within the reactor. This approach is expected to enhance the hyperthermic efficiency.

Acknowledgments

This work was funded by the Deutsche Forschungsgemeinschaft (DFG) project "GRK 2536". The authors gratefully acknowledge C. Schlundt and N. Schober for measuring XRD as well as S. Werner for measuring TEM, and A. Köppen for conducting the HR-TEM and EDX measurements. The authors thank the team of the element analysis centre for measuring inductively coupled plasma atomic emission spectroscopy. Furthermore, the authors would like to thank K.-W. Lei and W. Parak for the possibility of carrying out the hyperthermia measurements on their D5 series Calorimetry Coil-Set.

References

[1] Weißpflog, M.; Nguyen, N.; Sobania, N.; Hankiewicz, B. Non-Stoichiometric Cobalt Ferrite Nanoparticles by Green Hydrothermal Synthesis and their Potential for Hyperthermia Applications. *J. Phys Chem C* **2024**. DOI: 10.1021/acs.jpcc.4c03589

[2] Lucht, N.; Friedrich, R. P.; Draack, S.; Alexiou, C.; Viereck, T.; Ludwig, F.; Hankiewicz, B. Biophysical Characterization of (Silica-coated) Cobalt Ferrite Nanoparticles for Hyperthermia Treatment. *Nanomaterials* **2019**, *9* (12). DOI: 10.3390/nano9121713.

[3] Weißpflog, M.; Kabelitz, J.; Hankiewicz, B. *manuscript in preparation.*

Magnetic Particle Spectroscopy measurements with adjustable DC offset fields

F. Wolgast[1], E. Wendt[1], M. Schilling[1], F. Ludwig[1], and T. Viereck[1]

[1] *Institut für Elektrische Messtechnik und Grundlagen der Elektrotechnik (EMG) and LENA, TU Braunschweig, Braunschweig, Germany*

Introduction

The characterization of magnetic nanoparticles (MNPs) properties is essential to determine their suitability for the intended application. One interesting characterization method is the Magnetic Particle Spectroscopy (MPS), which uses a sinusoidal magnetic excitation field to periodically drive the MNPs into saturation. It is used both with and without an additional DC offset field to measure the dynamic nonlinear magnetization response. For example, this method is applied to investigate the suitability of MNPs for the imaging modality, the Magnetic Particle Imaging (MPI) [1], or it has recently been used for the evaluation of magnetic immunoassays (MIAs) based on the phase at a fixed DC offset field [2]. In addition to the phase, the harmonic ratio can also be used as a concentration-independent indicator for the detection of biological targets in MIAs. However, systematic investigations are necessary to understand the MNP behavior and to achieve the best performance in the end.

Methods

In order to fill this gap, MPS measurements with an adjustable DC offset field (ADOF) on different Brownian dominated particle systems and hydrodynamic sizes are carried out and evaluated in this work. To this end, the newly developed ADOF-MPS, shown in Figure 1, which operates at a fixed frequency of 2 kHz and a magnetic excitation field amplitude of 15 mT, is introduced. As particle systems self-synthesized singlecore cobalt-iron-zinc (CFZ14) particles as well as the from micromod commercially available multicore bionized nanoferrite (BNF80) particles with 80 nm hydrodynamic size and starch coating are investigated. Both exhibit Brownian relaxation behavior. The change in the hydrodynamic size is achieved by the functionalization of the particles with DNA strands.

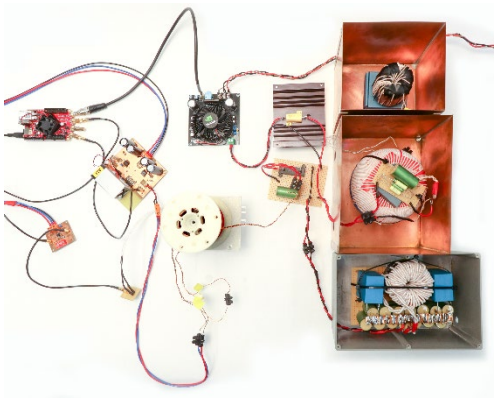

Figure 1: Setup of our new generation imunoMPS with the option to produce an ADOF.

Results

Figure 2 shows the measurement results on the CFZ14 particles containing the magnitudes of the second up to the fifth harmonic over the dc offset field. These MNPs have a small hydrodynamic size of around 27 nm leading to fast Brownian relaxation behaviour. It can be recognized that the even harmonics disappear in the absence of a DC offset field. Furthermore, the second harmonic shows the largest magnitude at approximately 9 mT and minima in the third and fifth harmonics are sharply defined. In comparison, Figure 3 shows the same spectrum for the BNF80 particles. It can be seen that the second harmonic also has the maximum amplitude, but the maximum is broader and lies at a greater field strength of 12 mT. The same can be said for the other higher harmonics, although the minima in particular are blurred and not as sharply defined as in the case for the CFZ14 particles. It should be noted that the relaxation of the BNF particles is significantly

slower due to the larger hydrodynamic size of 80 nm.

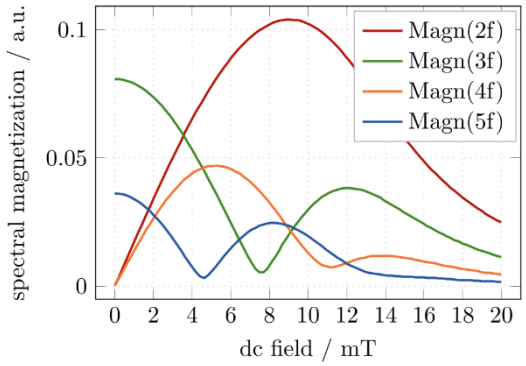

Figure 2: Magnitude measurement of the 2nd, 3rd, 4th and 5th harmonics of the CFZ14 particles for different DC offset fields.

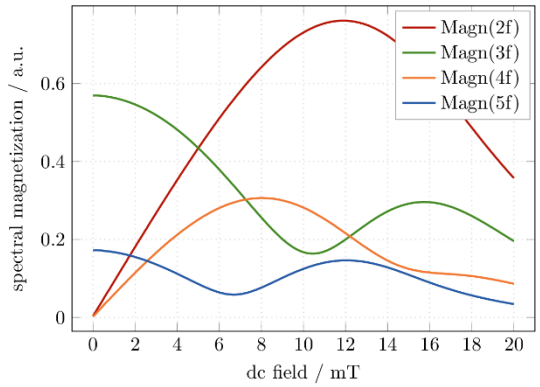

Figure 3: Magnitudes measurement of the 2nd, 3rd, 4th and 5th harmonics of the BNF80 particles for different DC offset fields.

In a next step we increased the hydrodynamic size of the CFZ14 particles to 37 nm by binding DNA strands with a length of 20 base pairs on their surface. Figure 4 shows the resulting ADOF spectrum for the magnitude of the second harmonic. While the magnitude of the harmonic decreases, a shift of the maximum to smaller dc offset field strengths of about 8.5 mT can be observed. The maximum change in the magnitude of the harmonic occurs at 12 mT and does not coincide with the maximum amplitude.

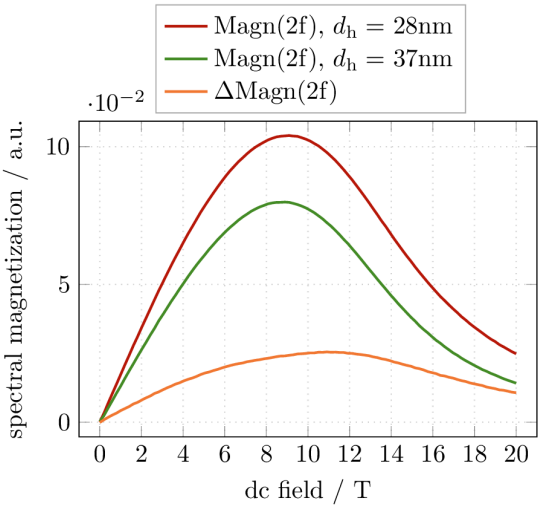

Figure 4: Measurement of the second harmonic magnitude of the CFZ14 particles for different DC offset fields and hydrodynamic sizes of 27 nm and 37 nm due to functionalizing with DNA strands.

In addition to this systematic investigation, Fokker-Planck simulations for Brownian relaxation were carried out in order to get a better overview of the DC field dependence for different hydrodynamic sizes and to investigate the influence of size distributions. Overall, the measurements compared to the simulation showing good agreement.

In a next step, the concentration independent harmonic ratios can be considered, which are of particular interest for the evaluation of MIAs.

Acknowledgments

This work was supported by the Deutsche Forschungsgemeinschaft (DFG, German Research Foundation) under the DFG Research Training Group 1952 Metrology for Complex Nanosystems as well as the DFG project VI 892/4-1. We also gratefully acknowledge the support by the Braunschweig International Graduate School of Metrology B-IGSM.

References

[1] S. Biederer et al., Magnetization response spectroscopy of superparamagnetic nanoparticles for magnetic particle. J. Phys. D: Appl. Phys., 42, pp. 205007, 2009

[2] P. Vogel et al., Critical Offset Magnetic Particle Spectroscopy for rapid and highly sensitive medical point-of-care diagnostics. Nat. Commun, 13, pp. 7230, 2022

List of Participants

Günter K. Auernhammer

Polymer Interfaces
Leibniz-Institut für Polymerforschung Dresden e.V.
Hohe Straße 6
01069 Dresden
Germany
Tel.: +49 351 4658 486
E-mail: auernhammer@ipfdd.de

Reza Azizmalayeri

Institute of Physical Chemistry and Polymer Physics, Department of Polymer Interfaces
Leibniz-Institut für Polymerforschung Dresden e. V.
Hohe Str. 6
01069 Dresden
Germany
Tel.: 0491781465773
E-mail: azizmalayeri@ipfdd.de

Tatiana Becker

Fachgebiet Mechanik Nachgiebiger Systeme
Technische Universität Ilmenau
Max-Planck-Ring 12
98693 Ilmenau
Deutschland
Tel.: 03677 / 69-1845
E-mail: tatiana.becker@tu-ilmenau.de

Silke Behrens

Institut für Katalyseforschung und -technologie
Karlsruher Institut für Technologie
Hermann-von-Helmholtz-Platz 1
76344 Eggenstein-Leopoldshafen
Deutschland
Tel.: 072160826512
E-mail: silke.behrens@kit.edu

Oksana Bilous

Computational and Soft Matter Physics
University of Vienna
Wehlistraße 65/6/34
1200 Vienna
Austria
Tel.: +380503905997
E-mail: oksana.bilous@univie.ac.at

Dmitry Borin

Chair of Magnetofluiddynamics, Measuring and Automation Technology
TU Dresden
George-Baehr-Str. 3
01062 Dresden
Germany
Tel.: 035146332307
E-mail: dmitry.borin@tu-dresden.de

Joachim Clement

Hematology and Internal Oncology
Jena University Hospital
Am Klinikum 1
07749 Jena
Germany
Tel.: 0049 3641 9 325820
E-mail: joachim.clement@med.uni-jena.de

Dietmar Eberbeck

Metrologie magnetischer Nanopartikel
Physikalisch-Technische Bundesanstalt
Abbestr. 2-12
10587 Berlin
Germany
Tel.: 03034817208
E-mail: dietmar.eberbeck@ptb.de

Manfred Ehresmann

Institute of Space Systems
University of stuttgart
Zentraler Rechnungseingang
Keplerstraße 7
70174 Stuttgart
Germany
Tel.: +49 711 685 69599
E-mail: ehresmann@irs.uni-stuttgart.de

Alexey Eremin

Nonlinear Phenomena
Institute of Physics, Otto von Guericke University
Universitätsplatz 2
39106 Magdeburg
Germany
Tel.: 03916750099
E-mail: alexey.eremin@ovgu.de

Lukas Fischer

Institut für Physik, Theorie der Weichen Materie / Biophysik
Otto-von-Guericke-Universität Magdeburg
Universitätsplatz 2
39106 Magdeburg
Germany
Tel.: +493916751703
E-mail: lukas.fischer@ovgu.de

Yashas Tejaskumar Gandhi

Institute for Computational Physics (ICP)
University of Stuttgart
Allmandring 3
70569 Stuttgart
Germany
Tel.: +4971168563593
E-mail: yashas-tejaskumar.gandhi@icp.uni-stutgart.de

Philipp Gebhart

Institute of Solid Mechanics
TU Dresden
George-Bähr-Straße 3c
01069 Dresden
Germany
Tel.: +49 351 463-39171
E-mail: philipp.gebhart@tu-dresden.de

Marina Grenzer

Material Theory and Modeling
Leibniz-Institut für Polymerfroschung Dresden
Hohe Strasse 6
01069 Dresden
Germany
Tel.: +49 351 4658 597
E-mail: grenzer@ipfdd.de

Yaser Hadadian

Metrology for magnetic nanoparticles
PTB
Abbestr. 2-12
10587 Berlin
Germany
Tel.: 03034817572
E-mail: yaser.hadadian@ptb.de

Birgit Hankiewicz

Physikalische Chemie
Universität Hamburg
Grindelallee 117
20146 Hamburg
Deutschlang
Tel.: 040428388347
E-mail: birgit.hankiewicz@uni-hamburg.de

Georg Herdrich

Institute of Space Systems
University of stuttgart
Zentraler Rechnungseingang
Keplerstraße 8
70175 Stuttgart
Germany
Tel.: +49 711 685 62412
E-mail: herdrich@irs.uni-stuttgart.de

Noor Jahan

Physics and Astronomical sciences
Central university of Himachal Pradesh
Shahpur university
176206 Kangra
India
Tel.: 06005781006
E-mail: noor.jahan@hpcu.ac.in

Karl Kalina

Faculty of Mechanical Science and Engineering
Institute of Solid Mechanics / TU Dresden
George-Bähr-Straße 3c
01069 Dresden
Germany
Tel.: +49 351 463-33284
E-mail: karl.kalina@tu-dresden.de

Jens Kirchner

Elektrotechnik-Elektronik-Informationstechnik
Friedrich-Alexander-Universität Erlangen-Nürnberg (FAU)
Cauerstr. 9
91058 Erlangen
Germany
Tel.: +49 160 95082599
E-mail: jens.kirchner@fau.de

Juri Kopp

Physics
University of Duisburg-Essen
Lotharstraße 1
47057 Duisburg
Germany
Tel.: +49 203-379-2955
E-mail: juri.kopp@uni-due.de

Martin Krichler

Project Management
Bilfinger Nuclear & Energy Transistion GmbH
Alfred-Nobel-Str. 20
97080 Würzburg
Germany
Tel.: +499319036238
E-mail: martin.krichler@bilfinger.com

Ali Lakkis

Experimental physics 5
Universität Bayreuth
Universitätsstraße 30
95447 Bayreuth
Deutschland
Tel.: 00491731728566
E-mail: Ali.Lakkis@uni-bayreuth.de

Joachim Landers

Faculty of Physics
University of Duisburg-Essen
Lotharstr. 1
47057 Duisburg
Germany
Tel.: +49 203 379 2384
E-mail: joachim.landers@uni-due.de

Adrian Lange

Lehrstuhl für Magnetofluiddynamik, Mess- und Automatisierungstechnik
TU Dresden
George-Bähr-Straße 3
01062 Dresden
BRD
Tel.: 0351-46334703
E-mail: adrian.lange@tu-dresden.de

Zhenzhen Liu

Mechatronic Engineering
Technical University Dresden
George-Bähr-Street 3
01062 Dresden
Germany
Tel.: 01624054475
E-mail: zhenzhen.liu@mailbox.tu-dresden.de

Stefan Lyer

Sektion für experimentelle Onkologie und Nanomedizin
Universitätsklinikum Erlangen
Glückstraße 10a
91054 Erlangen
Deutschland
Tel.: 091318533142
E-mail: stefan.lyer@uk-erlangen.de

Andreas Menzel

Institut für Physik
Otto-von-Guericke-Universität Magdeburg
Universitätsplatz 2
39106 Magdeburg
Germany
Tel.: 0391/6757490
E-mail: a.menzel@ovgu.de

Hajnalka Nádasi

Institute of Physics
Otto von Guericke University Magdeburg
Universitätsplatz 2
39106 Magdeburg
Germany
Tel.: 03916750098
E-mail: hajnalka.nadasi@ovgu.de

Stefan Odenbach

Magnetofluiddynamics, Measuring and Automation Technology
TU Dresden
George-Bähr-Str. 3
01069 Dresden
Germany
Tel.: 035146332062
E-mail: stefan.odenbach@tu-dresden.de

Moritz Raphael

Chemistry
Universität zu Köln
Greinstraße 6-8
50939 Cologne
Germany
Tel.: +49 221 470 5472
E-mail: moritz.raphael@uni-koeln.de

Ingo Rehberg

Experimental Physics
University of Bayreuth
Grace-Hopper-Straße 3a
23562 Lübeck
Germany
Tel.: 0451 48900475
E-mail: Ingo.Rehberg@uni-bayreuth.de

Marius Reiche

Mechanics of Compliant Systems Group
Technische Universität Ilmenau
Max-Planck-Ring 12
98693 Ilmenau
Deutschland
Tel.: 03677691884
E-mail: marius.reiche@tu-ilmenau.de

Reinhard Richter

Experimentalphysik 5
University of Bayreuth
Universitätsstrasse 30
95447 Bayreuth
Germany
Tel.: 0921-553311
E-mail: reinhard.richter@uni-bayreuth.de

Mehran Roghani

Institute theory of polymer
Leibniz-Institut für Polymerforschung Dresden e. V.
Hohe str. 6
01069 Dresden
Germany
Tel.: +4935146581220
E-mail: Roghani@ipfdd.de

Dirk Romeis

Materialtheorie und Modellierung
Leibniz-Institut für Polymerforschung Dresden e.V.
Hohe Strasse 6
01069 Dresden
Germany
Tel.: 035146581115
E-mail: romeis@ipfdd.de

Heinrich Roth

IFKM
TU Dresden
George-Bähr-Straße 3c
01069 Dresden
Germany
Tel.: +49 351 463-33450
E-mail: heinrich_tristan.roth@mailbox.tu-dresden.de

Annette Schmidt

Chemistry Department
Universität zu Köln
Greinstr. 4 - 6
50939 Köln
D
Tel.: +49 (0)221 470 5410
E-mail: annette.schmidt@uni-koeln.de

Patrick Schütz

Institut für Physikalische Chemie
Universität Hamburg
Grindelallee 117
20146 Hamburg
Germany
Tel.: +49 40 42838-9952
E-mail: patrick.schuetz@uni-hamburg.de

Rebecca Stephan

Institute for Computational Physics
University of Stuttgart
Neckarstraße 210
70190 Stuttgart
Germany
Tel.: 0157506444372
E-mail: rebecca.stephan@icp.uni-stuttgart.de

Thilo Viereck

Institut für Elektrische Messtechnik und Grundlagen der Elektrotechnik (EMG)
TU Braunschweig
Hans-Sommer-Straße 66
38106 Braunschweig
DE
Tel.: 0531 391-3860
E-mail: t.viereck@tu-braunschweig.de

Thomas Wallmersperger

Maschinenwesen
IFKM/TU Dresden
George-Bähr-Str. 3c
01069 Dresden
Germany
Tel.: +49 351 463-37013
E-mail: thomas.wallmersperger@tu-dresden.de

Andreas Weidner

Fachgebiet Elektrochemie und Galvanotechnik
TU Ilmenau
Gustav-Kirchhoff-Strasse 6
98693 Ilmenau
Deutschland
Tel.: 015739065010
E-mail: andreas.weidner@tu-ilmenau.de

Florian Wolgast

Institut für elektrische Messtechnik und
Grundlagen der Elektrotechnik
TU Braunschweig
Hans-Sommer-Str. 66
38106 Braunschweig
Germany
Tel.: 0531 391 3876
E-mail: f.wolgast@tu-bs.de